



Joint parameter-input estimation for virtual sensing on an offshore platform using output-only measurements

Mingming Song^a, Silas Christensen^b, Babak Moaveni^{a,*}, Anders Brandt^c, Eric Hines^a

^a Dept. of Civil and Environmental Engineering, Tufts University, Medford, MA, USA

^b Dept. of Technology and Innovation, University of Southern Denmark, Odense, Denmark

^c Dept. of Mechanical and Production Engineering, Aarhus University, Aarhus, Denmark

ARTICLE INFO

Keywords:

Offshore platform
Structural health monitoring
Recursive Bayesian inference
Input estimation
Virtual sensing

ABSTRACT

This paper presents a recursive Bayesian inference framework for joint parameter-input identification, and virtual sensing for strain time history prediction of an offshore platform using sparse output-only measurements. The studied offshore platform, known as FINO3, is in the North Sea and is instrumented with a variety of sensors, including accelerometers and strain gauges. Offshore platforms are fatigue critical structures due to harsh marine environmental conditions and continuous cyclic wind and wave loads. Therefore, continuous monitoring of strain time histories at hotspot locations of offshore structures is important for reducing maintenance cost and avoiding unexpected failures. A windowed unscented Kalman filter (UKF) is employed to estimate an uncertain modeling parameter (foundation stiffness) and unknown input load time histories using output-only acceleration and strain measurements. The input loads are divided into overlapping windows, and windowed inputs and model parameters are combined as an augmented state vector in the UKF framework. Then strain time histories at critical locations are estimated through a virtual sensing strategy using the estimated input loads and model parameter. A traditional modal expansion approach combined with model updating is also implemented for the purpose of verification and comparison. The proposed method is first demonstrated through a numerical study using a finite element model of FINO3, where accurate model parameter and input estimations are obtained. Then the approach is further investigated using the actual measurements on FINO3. More accurate strain predictions are provided by the UKF than the modal expansion approach, which recommends the proposed UKF method for fatigue monitoring and input estimation.

1. Introduction

Offshore structures are subject to harsh marine environmental conditions and continuous cyclic loading, including wind and wave loads, making them fatigue critical structures. Based on a report by Röckmann et al. [1], the operational and maintenance cost of offshore wind turbines accounts for 25–30% of their life cycle cost. Therefore, condition monitoring of offshore structures can provide substantial safety and financial benefits. Fatigue life of metallic structures can be estimated using strain measurements at locations of interest also known as hotspots. However, sensor placement at all hotspot locations in offshore structures are often too expensive or

* Corresponding author.

even prohibitive in some cases when they are not accessible. Virtual sensing has been proposed for estimating quantities of interest such as strains at hotspots using sparse measurements at accessible locations on the structure [2–4]. Since only sparse sensors at accessible locations are required for virtual sensing, the instrumentation cost can be significantly reduced.

Virtual sensing is often implemented using experimentally identified mode shapes combined with a numerical model, e.g., finite element (FE) model [5,6]. Papadimitriou et al. proposed a fatigue estimation method in metallic structures based on predicted power spectral density using a Kalman filter (KF) [7]. Lliopoulos et al. performed acceleration and strain predictions of a 3 MW offshore wind turbine in Belwind wind farm using virtual sensing strategy under different environmental and operational conditions, including parked/idling case, run-up, fully rotating, rotor stop-start cycle, and long-term operation case [8,9]. Maes et al. focused on dynamic strain estimation and compared the performance of KF, joint input-state estimation, and modal expansion approaches using experimental data for a 3 MW offshore monopile wind turbine on parked and rotating conditions [10]. Skaftø et al. proposed a modal decomposition approach for strain estimation of a laboratory scaled model of an offshore structure where a Ritz vector was used for quasi-static response and experimental mode shapes were used for dynamic response [11]. Hankel et al. performed a numerical study of strain estimation for offshore wind turbines with jacket substructures using a dual-band modal expansion approach [12]. Tarpø et al. implemented strain estimation using a modal expansion method for a scaled offshore platform in a laboratory where the performances of mode shapes from an FE model and expanded experimental mode shapes are compared [13]. When an FE model is utilized to infer the full-field mode shapes in a modal expansion approach, the accuracy of virtual sensing depends on the accuracy of the model, and therefore, model updating can be employed to calibrate the model and reduce model uncertainties. Model updating is a process of fusing measurements and a numerical model to estimate uncertain model parameters and improve model predictions. This approach is also referred to as model calibration. Giagopoulos et al. performed stress predictions using an updated large-scale high-fidelity FE model of a lignite grinder, where fatigue life estimation was verified by an observed crack in the real structure [14]. Kullaa [15] combined Bayesian empirical and analytical virtual sensing to estimate full-field response of a numerical frame structure. In this approach, less noisy estimates of actual measurements were first obtained through Bayesian empirical virtual sensing and then used for modal expansion, which provided more accurate predictions than directly using actual measurements.

Traditionally, model updating is performed by updating uncertain parameters of a model through minimizing an objective/loss function which is defined as the misfit between model-predicted and measured response. Numerous applications of model updating on large-scale real-world structures have been performed with reasonable successes [16–23]. Drawbacks of model updating based on optimization include lack of uncertainty quantification for model parameters and inaccurate results in unidentifiable problems where no single global optimum exists. These drawbacks can be overcome by applying Bayesian inference where the posterior probability distribution of updating parameters is obtained by integrating the prior knowledge of uncertain model parameters with the likelihood of measurements. Bayesian model updating can be performed in a batch or recursive manner. In the batch case, all the available measurements are included in the likelihood to derive the final posterior distribution [24–31]. In the recursive case, only the latest measured data are used in a sequential inference approach and a series of posterior distributions are generated at different time steps. Compared to the batch approach, the recursive Bayesian method has the benefit of updating a posterior distribution in a near real-time fashion by fusing new measurements consecutively. Common recursive Bayesian estimation methods include KF, extended KF (EKF) [32,33], unscented KF (UKF) [34], and particle filtering (PF) [34,35]. Chatzi and Smyth compared the performance of UKF and PF for nonlinear model updating of a three degree-of-freedom system with Bouc-Wen hysteretic behavior using non-collocated heterogeneous data [34]. Astroza et al. applied UKF for nonlinear model updating of civil structures [36] and seismic input estimation [37] in order to study the effect of modeling errors on model updating [38]. The effect of modeling errors can be alleviated by an adaptive KF proposed by Song et al. where the noise variance is updated along with model parameters [39]. Erazo et al. performed nonlinear model updating and state estimation of a full-scale seven-story shear wall structure tested on a shake table using UKF [40].

The input loads are not required to be measured/known for strain estimations using the modal expansion approach. Information regarding the input time history is valuable, however, for structural design or assessment of structural conditions in similar environments. Some methods have been developed for input estimation which can be classified into direct methods, regularization methods, and probabilistic methods [41]. Lourens et al. employed an augmented KF (AKF) for force identification of a laboratory steel beam and compared their results to a classical deterministic method [42], finding that AKF provided more accurate results for collocated cases because it accounts for modeling errors. In another study, they performed joint input-state estimation of a laboratory steel beam and a real-world footbridge [43]. The algorithm was modified from the method proposed by Gillijns and De Moor [44] which has the structure of KF except that the true value of the input was replaced by an optimal estimate. A similar EKF with unknown input algorithm was developed by Liu et al. for joint state-parameter-input estimation where displacement data were fused with accelerations to avoid drift in the identified input [45]. Azam et al. developed a dual KF for joint state-input estimation and compared its performance with AKF [42] and the filter of Gillijns and De Moor [44] on a laboratory frame structure [46,47]. Zhang et al. proposed a Bayesian force reconstruction approach which considers both measurement noise and model uncertainty based on transfer function and applied it to an experimental beam where a credible interval of force estimation was obtained [48]. Ebrahimian et al. completed joint parameter-seismic input estimation using EKF on a nonlinear reinforced concrete building model where ground excitation forces were divided into windows with overlapping [49]. They further applied the windowed EKF approach for strain estimation of an offshore wind turbine (OWT) and compared with a modal expansion approach [50]. Naets et al. proposed an AKF for joint state-input-parameter estimation using parametric model order reduction to increase computation efficiency [51]. Pahn et al. developed an input estimation algorithm in frequency domain using a frequency response function and verified it through a numerical offshore wind turbine study in which both wind and wave loads were estimated [52]. Recently, a substructure-based framework for input-state estimation using AKF was developed by Tatsis et al. and was illustrated numerically using three wind turbine substructures [53].

In this paper, a recursive Bayesian inference method, based on UKF, is employed to estimate the model parameter and unknown

input loads using output-only measurements of the FINO3 offshore structure. The input loads at consecutive time windows are concatenated with the model parameters to form the augmented state vectors which are updated sequentially using acceleration measurements. Then the strain estimations at locations of interest are computed using the estimated parameter and input loads. For the purpose of verification, these results are compared to those of a traditional modal expansion approach combined with model updating, as well as the actual strain measurements. The novelties of this study include an improved joint parameter-input estimation using a windowed UKF method, as well as its application to a unique set of experimentally measured data on a real-world offshore structure.

2. Virtual sensing methodology

In this section, subsection 2.1 provides details of the UKF-based recursive Bayesian inference method for joint estimation of model parameters and unknown input loads using output-only measurements. Subsection 2.2 provides a review of the traditional modal expansion approach combined with model updating.

2.1. UKF-based recursive Bayesian inference for joint parameter-input estimation

The state space formulation of dynamic systems for parameter estimation [39] is modified below for the purpose of joint parameter-input estimation:

$$\begin{cases} \boldsymbol{\psi}_{k+1} = \boldsymbol{\psi}_k + \mathbf{w}_k & \mathbf{w}_k \sim N(\mathbf{0}, \mathbf{Q}_k) \\ \mathbf{y}_{k+1} = \mathbf{h}_{k+1}(\boldsymbol{\psi}_{k+1}) + \mathbf{v}_{k+1} & \mathbf{v}_{k+1} \sim N(\mathbf{0}, \mathbf{R}_{k+1}) \end{cases} \quad (1)$$

in which $\boldsymbol{\psi}_k$ is the augmented state vector at time window k and consists of model parameters $\boldsymbol{\theta}_k$ and input load \mathbf{f}_k : $\boldsymbol{\psi}_k = [\boldsymbol{\theta}_k^T \ \mathbf{f}_k^T]^T$. Note that the input load is divided into N overlapping windows and the augmented state includes the input time history in the current window, while the input signal in previous windows is kept fixed as their estimated values. The purpose of overlaps between windows is to improve the input estimation accuracy. \mathbf{y}_{k+1} collects the measurements of all channels at time steps in window $k+1$, and $\mathbf{h}_{k+1}(\boldsymbol{\psi}_{k+1})$ denotes the response of the numerical model with parameters $\boldsymbol{\theta}_{k+1}$ and input load \mathbf{f}_{k+1} . In Eq. (1), the augmented state is modeled as a random walk process. Vectors \mathbf{w}_k and \mathbf{v}_{k+1} contain the process noise and measurement noise which follow a zero-mean Gaussian distribution with covariance matrices \mathbf{Q}_k and \mathbf{R}_{k+1} , respectively. The values of \mathbf{Q}_k and \mathbf{R}_{k+1} can change for different time windows. Adaptive KF algorithms were proposed with \mathbf{Q}_k and/or \mathbf{R}_{k+1} estimated and updated over time steps [39,54], however, their values are kept constant in this study. The covariance matrix of process noise \mathbf{Q} is set to be a small positive value in order to facilitate the convergence of the augmented state. It is worth noting that a fixed \mathbf{Q} is not appropriate if the inputs are highly non-stationary and their amplitudes change drastically. In this case, an adaptive KF where \mathbf{Q} is updated sequentially may be preferred [55,56], or alternatively, the input normalization can be modified for different windows accordingly.

Table 1

UKF algorithm for joint parameter-input estimation.

Step 0: Initializing State Vector and Covariance Matrix

$\boldsymbol{\psi}_0 = [\boldsymbol{\theta}_0^T \ \mathbf{f}_0^T]^T$, \mathbf{P}_0 . Here $\boldsymbol{\theta}_0$ is the vector of initial value of model parameters and \mathbf{f}_0 denotes initial value of input load in the first window and is assumed to be zero, i.e., $\mathbf{f}_0 = \mathbf{0}$.

Loops for windows: $k = 0, 1, 2, 3, \dots, N-1$

Step 1: Prediction Step

(1.0) For window $k \geq 1$, initialize input load in state vector $\boldsymbol{\psi}_k = [\boldsymbol{\theta}_k^T \ \mathbf{f}_k^T]^T$: $\mathbf{f}_k = [(\mathbf{f}_{k-1}^T \ \mathbf{0}^T)^T]$ in which \mathbf{f}_{k-1}^T denotes the overlapping part of input in previous window $k-1$ which has been estimated and used here for initial values. The rest of the load in the current window is assumed to be zero.

(1.1) $\boldsymbol{\psi}_{k+1}^- = \boldsymbol{\psi}_k$, $\mathbf{P}_{k+1}^- = \mathbf{P}_k + \mathbf{Q}$

(1.2) Generate sigma points (SP): $\boldsymbol{\Psi}_{k+1|k} = [\boldsymbol{\psi}_{k+1}^- \ \boldsymbol{\psi}_{k+1}^- + \gamma\sqrt{\mathbf{P}_{k+1}^-} \ \boldsymbol{\psi}_{k+1}^- - \gamma\sqrt{\mathbf{P}_{k+1}^-}]$

(1.3) Evaluate predictions at SP: $\mathcal{Y}_{k+1|k} = \mathbf{h}_{k+1}(\boldsymbol{\Psi}_{k+1|k})$

(1.4) Mean of predictions: $\mathbf{y}_{k+1}^- = \sum_{i=1}^{2n_p+1} \mathbf{W}_m^{(i)} \mathcal{Y}_{k+1|k}^{(i)}$

Step 2: Correction Step

(2.1) $\mathbf{P}_{y_{k+1}|y_{k+1}} = \sum_{i=1}^{2n_p+1} \mathbf{W}_c^{(i)} [\mathcal{Y}_{k+1|k}^{(i)} - \mathbf{y}_{k+1}^-] [\mathcal{Y}_{k+1|k}^{(i)} - \mathbf{y}_{k+1}^-]^T + \mathbf{R}$

(2.2) $\mathbf{P}_{\boldsymbol{\psi}_{k+1}|y_{k+1}} = \sum_{i=1}^{2n_p+1} \mathbf{W}_c^{(i)} [\boldsymbol{\Psi}_{k+1|k}^{(i)} - \boldsymbol{\psi}_{k+1}^-] [\mathcal{Y}_{k+1|k}^{(i)} - \mathbf{y}_{k+1}^-]^T$

(2.3) Kalman gain: $\mathbf{K}_{k+1} = \mathbf{P}_{\boldsymbol{\psi}_{k+1}|y_{k+1}} (\mathbf{P}_{y_{k+1}|y_{k+1}})^{-1}$

(2.4) State vector update: $\tilde{\boldsymbol{\psi}}_{k+1} = \boldsymbol{\psi}_{k+1}^- + \mathbf{K}_{k+1} (\mathbf{y}_{k+1} - \mathbf{y}_{k+1}^-)$

(2.5) State uncertainty update: $\tilde{\mathbf{P}}_{k+1} = \mathbf{P}_{k+1}^- - \mathbf{K}_{k+1} \mathbf{P}_{y_{k+1}|y_{k+1}} \mathbf{K}_{k+1}^T$

Step 3: Convergence Test

(3.1) Evaluate relative change of augmented state: $\Delta\boldsymbol{\psi} = |\tilde{\boldsymbol{\psi}}_{k+1} - \boldsymbol{\psi}_{k+1}^-|/|\boldsymbol{\psi}_{k+1}^-|$

(3.2) Compare it with convergence criterion ε

If $\Delta\boldsymbol{\psi} \leq \varepsilon$, assign $\boldsymbol{\psi}_{k+1} = \tilde{\boldsymbol{\psi}}_{k+1}$, $\mathbf{P}_{k+1} = \tilde{\mathbf{P}}_{k+1}$ and go to next window with $k = k+1$

If $\Delta\boldsymbol{\psi} > \varepsilon$, repeat from step (1.1) with $\boldsymbol{\psi}_k = \tilde{\boldsymbol{\psi}}_{k+1}$, $\mathbf{P}_k = \tilde{\mathbf{P}}_{k+1}$

End loop for k

KF methods are often performed recursively at each time step, i.e., the state vector gets updated using a new measurement at each time step. Special treatments and transformations are needed to implement the proposed windowing strategy in this study. Here the measurement y_{k+1} is equal to $\left[(y_{k+1}^1)^T \dots (y_{k+1}^m)^T \right]^T$ in which y_{k+1}^m refers to the measurements of channel m in window $k + 1$. Suppose the window size is L , then the size of y_{k+1} is $mL \times 1$. The covariance matrix Q consists of the respective process noise covariance of model parameters and input load as $Q = \text{diag}(Q^\theta, Q^f)$ which has the size of $(n_\theta + L) \times (n_\theta + L)$ where n_θ is the dimension of θ . Let $R^0 = \text{diag}([R_1 \dots R_m])$ denote the covariance of measurement noise for all m channels. Then the matrix R in Eq. (1) is formulated as $R = \text{diag}([R_1 \mathbf{1}_{1 \times L} \dots R_m \mathbf{1}_{1 \times L}])$ where $\mathbf{1}_{1 \times L}$ denotes a $1 \times L$ vector of ones. It is worth noting that, if multiple input load time histories are to be estimated, as has been done in this study, then all the unknown input loads can be concatenated in the augmented state, e.g., $\psi_k = [\theta_k^T \ f_k^T \ p_k^T]^T$ where p denotes another independent input. In this case the matrix Q has to be changed accordingly, but the formulation of the matrix R remains the same. Similarly, when multiple input time histories are strongly non-stationary and their amplitudes change drastically, an adaptive KF where Q is updated sequentially [55,56], or an adaptive input normalization strategy can be applied.

The considered structural system is assumed to be linear elastic in this study, however, the joint estimation of model parameters and input loads becomes a nonlinear Bayesian filtering problem. The linear elastic assumption of the studied structure is confirmed by the small vibration amplitude and the consistency of identified modal parameters. It is worth noting that the proposed joint parameter-input algorithm does not require the structure to be linear elastic, and a nonlinear model can be employed using the exact same UKF framework. EKF and UKF are the most popular nonlinear recursive Bayesian estimation algorithms, and UKF is selected in this study for its high accuracy and computational efficiency. Steps of the UKF algorithm for joint parameter-input estimation are presented in Table 1. It is worth noting that the initial value of input loads in each window is assumed to be zero. Overlapping parts between windows, however, use initial values estimated in the previous window. However, unlike the state vector ψ_k , the initial covariance matrix P_0 which consists of two parts, i.e., $P_0 = \text{diag}(P_0^\theta, P_0^f)$, is only initialized for the first window and then updated at each window (Steps (1.1) and (2.5)). This means that the initial covariance for latter windows is equal to the posterior covariance from previous windows, even though the input loads change in different windows. This strategy has been shown to work better than initializing covariance for new input loads in each window, which can cause the divergence of input estimations as observed by the authors in a preliminary study. Other setting parameters for UKF are described below: at step (1.2), $\gamma = \sqrt{n_\psi + \lambda}$ where n_ψ is the dimension of ψ and λ is a scaling parameter and is equal to $\alpha^2(n_\psi + \kappa) - n_\psi$; κ is a secondary scaling parameter which is usually set to 0 or $3 - n_\psi$ such that the kurtosis of the sigma points (SP) agrees with that of the Gaussian distribution [57]; α determines the spread of SP and is usually set to a small positive value $0.0001 \leq \alpha \leq 1$. A smaller α reduces the variation of prediction covariance caused by higher order term effects [58]. At steps (1.4), (2.1), and (2.2), the weights $W_m^{(i)}$ and $W_c^{(i)}$ are determined as

$$W_m^{(1)} = \lambda / (n_\psi + \lambda), \quad W_c^{(1)} = \lambda / (n_\psi + \lambda) + (1 - \alpha^2 + \beta) \quad (2)$$

$$W_m^{(i)} = W_c^{(i)} = 0.5 / (n_\psi + \lambda) \quad i = 2, \dots, 2n_\psi + 1 \quad (3)$$

Parameter β incorporates prior knowledge about distribution of the state vector, and its optimal value is equal to 2 for Gaussian distribution [58]. In this study, the parameter values are selected as $\kappa = 0$, $\alpha = 0.1$, and $\beta = 2$. In general, the effects of these parameters on filter performance are small, as long as they are selected in the recommended range. At step (3.2), the convergence criterion should be adjusted for each application to balance the estimation accuracy versus the computational effort.

2.2. Modal expansion combined with model updating

In this approach, a numerical model (e.g., FE model) is first updated using the measured data, then quantities of interest such as strain time histories are estimated using complete mode shapes obtained from the calibrated model. By integrating the model with measurements, uncertainty of model parameters can be reduced, and therefore, model predictions are improved. In this study, a traditional deterministic model updating approach is implemented, in which updating parameters are estimated through optimization by minimizing the following objective/cost function [23]:

$$f(\theta) = r(\theta)^T W_r(\theta) + (\theta - \theta_0)^T W_\theta(\theta - \theta_0) \quad (4)$$

where θ_0 is the initial/prior value of model parameters, and $r(\theta)$ denotes the residual vector which consists of two parts: natural frequencies residual $r_f(\theta)$ and mode shapes residual $r_s(\theta)$ which are defined as:

$$r_f^i(\theta) = \frac{\lambda_i(\theta) - \tilde{\lambda}_i}{\tilde{\lambda}_i} \quad (5)$$

$$r_s^i(\theta) = \frac{\Phi^i(\theta)}{\Phi_r^i(\theta)} - \frac{\tilde{\Phi}^i}{\tilde{\Phi}_r^i} \quad (6)$$

$\lambda_i(\theta)$ and $\tilde{\lambda}_i$ refer to the model-predicted eigenfrequency of mode i ($\lambda_i(\theta) = (2\pi f_i(\theta))^2$) in which $f_i(\theta)$ is natural frequency in Hz) and

its identified counterpart from measured data, respectively, while $\Phi^i(\theta)$ and $\tilde{\Phi}^i$ are the corresponding mode shapes. The subscript r denotes the reference channel for normalizing mode shapes, which can be selected as the channel with the largest absolute component. Note that the numerical models usually have a large number of degrees of freedom (DOFs), and $\Phi^i(\theta)$ should only include the DOFs corresponding to the measurement locations. W is a diagonal weight matrix for different modes, e.g., smaller weights are usually assigned to modes with higher identification uncertainty. When equal weights are assigned for all modes, W becomes $\text{diag}([\mathbf{1}_{1 \times n_m} \quad 1/m \mathbf{1}_{1 \times mn_m}])$ where $\mathbf{1}_{1 \times n_m}$ denotes a $1 \times n_m$ vector of ones with n_m being the number of modes used in model updating, and m is the number of measurement channels. W_θ is a regularization weight matrix which applies penalty to the changes in θ . The second term in Eq. (4) is a regularization term which helps to prevent ill-conditioning of the inverse problem and is similar to the use of prior distribution in the Bayesian model updating. In this study, W_θ is set to $\text{diag}(0.01 \mathbf{1}_{1 \times n_\theta})$ [23,59].

After the model is calibrated and the optimal values of updating parameters θ^{opt} are obtained, the complete mode shapes of the calibrated model are used to estimate the quantities of interest such as strains, through modal expansion [8].

$$\begin{bmatrix} u(t) \\ \varepsilon(t) \end{bmatrix} = \begin{bmatrix} \Phi_u(\theta^{opt}) \\ \Phi_\varepsilon(\theta^{opt}) \end{bmatrix} q(t) \quad (7)$$

In this equation, $u(t)$ refers to displacement measurements at time t , $\varepsilon(t)$ are unknown strains of interest, $\Phi_u(\theta^{opt})$ and $\Phi_\varepsilon(\theta^{opt})$ are the displacement mode shape matrix at measured DOFs and the strain mode shape matrix at locations of interest, respectively. The strain mode shapes should be computed from the model (e.g., using the FE model and the Hermite shape function for beam element) [60]. Each column of the strain mode shape matrix $\Phi_\varepsilon(\theta^{opt})$ consists of the strains at locations of interest when the structure has the deformation of the corresponding displacement mode shape. It is worth noting that displacement data can be actual displacement measurements or obtained by numerically integrating the acceleration data. However, the double-integration of accelerations will cause numerical errors especially at low frequencies where integrated displacements may get distorted. Therefore, the integration strategy will only provide accurate estimates of dynamic strain at high frequencies. In this case, the low frequency contents (quasi-static) of strain estimations can be estimated from available strain gauges or other type of displacement sensors, e.g., linear variable differential transformers (LVDTs) and string pots. The total strain estimations are then obtained as the summation of dynamic and quasi-static estimates. This strategy has been employed in this paper. Vector $q(t)$ is the response at modal coordinates which can be estimated using the measured response and the top part of Eq. (7):

$$\hat{q}(t) = \Phi_u^+ u(t) \quad (8)$$

in which Φ_u^+ denote the Moore-Penrose inverse (pseudo-inverse) of Φ_u with the size of $m \times n_m$. Note that number of measurements cannot be smaller than the number of modes considered ($m \geq n_m$) to ensure unique solution of $q(t)$. Strains at the location of interest are then estimated using the obtained modal coordinates and the bottom part of Eq. (7):

$$\hat{\varepsilon}(t) = \Phi_\varepsilon \hat{q}(t) \quad (9)$$

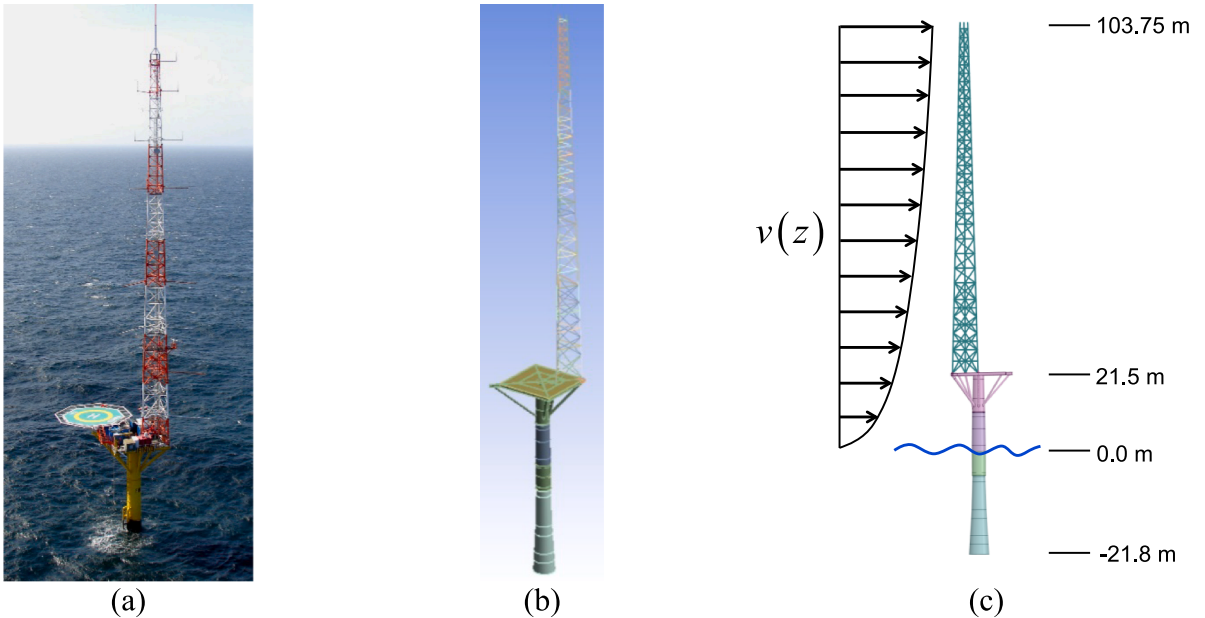


Fig. 1. (a) FINO3 platform; (b) illustration of FE model; (c) power law profile of wind speed.

3. FINO3 structure and measured/simulated data

The considered structure is an offshore research platform located in the North Sea referred to as FINO3, shown in Fig. 1(a) [61]. The platform has been instrumented with 12 accelerometers (A1 – A12) and 3 strain gauges (S1, S2 and S3). The layout of sensors is illustrated in Fig. 2. The symbols in parentheses in Fig. 2(a) denote the directions of acceleration measurements, and a total of 24 channels of accelerations are collected. The numerical study of joint parameter-input estimation is based on the FE model of the FINO3, which is illustrated in Fig. 1(b). The FE model is built in OpenSees, an open-source FE analysis software [62]. The monopiles, platforms and the columns of the mast are modeled using beam-column elements, and the braces of the mast are modeled as truss elements. The whole structure is made of steel with a nominal Young's modulus of 205 GPa. The damping property of the structure is assumed to be Rayleigh damping with damping ratios of 0.9% for mode 2 and 1.1% for mode 4. These damping ratios are based on the identified modal properties using actual measurements. It is worth noting that the damping properties of offshore structures can be time-variant, amplitude-dependent, and affected by soil-structure interactions. However, for the current FINO3 structure, the damping properties are observed to be generally stable at different times based on the system identification results. This is most likely because the upper part of FINO3 is a truss structure which has limited aerodynamic effects, unlike offshore wind turbines with significant aerodynamic effects in which the damping in fore-aft direction can change drastically as a function of wind speed. Including additional updating parameters for damping properties would be more appropriate for applications with significant aerodynamic effects and/or soil-structure interactions. A sensitivity analysis is performed to study the effects of soil stiffness at the foundation, which are modeled by three springs, a lateral spring with stiffness k_L , a vertical support spring with stiffness k_V and a rotational spring with stiffness k_R . It is found that only the rotational spring made a meaningful contribution to the first few modes of the structure. Since the stiffness of steel materials has relatively small uncertainty, the foundation stiffness k_R is chosen as the only updating parameter, i.e., $\theta = [k_R/k_R^0]$ in which k_R^0 denotes the initial value. Based on previous studies, the initial rotational stiffness is assumed to be 25 GN/rad [50,63].

The FINO3 structure is assumed to be excited only by wind load and the effect of wave load is not considered in this study. The structure has a height of over 100 m above sea level with the first bending mode at 0.42 Hz, therefore, it is believed that the main excitation force comes from wind load, and the wave load plays a less important role because it only contains relatively low frequency contents around 0.1 Hz [64]. The estimated input can be seen as the equivalent load of combined effects of wind and wave loads. It is worth noting that the quasi-static part of the wave load is not identifiable because no sensor is available below the sea level, although its dynamic part can be potentially estimated using acceleration data above the sea level. However, the dynamic band in this study is over 0.25 Hz, which is above the dominant frequency of the wave load (<0.1 Hz), therefore, the dynamic part of the wave load is relatively small and adds limited information to the dynamic response. The joint estimation of wind load along with wave load will be a future research topic. The wind speed is assumed to follow the Kaimal spectrum as described below [64]:

$$S_{vv}(f) = \frac{\sigma_v^2(4L/\bar{v})}{(1 + 6fL/\bar{v})^{5/3}} \quad (10)$$

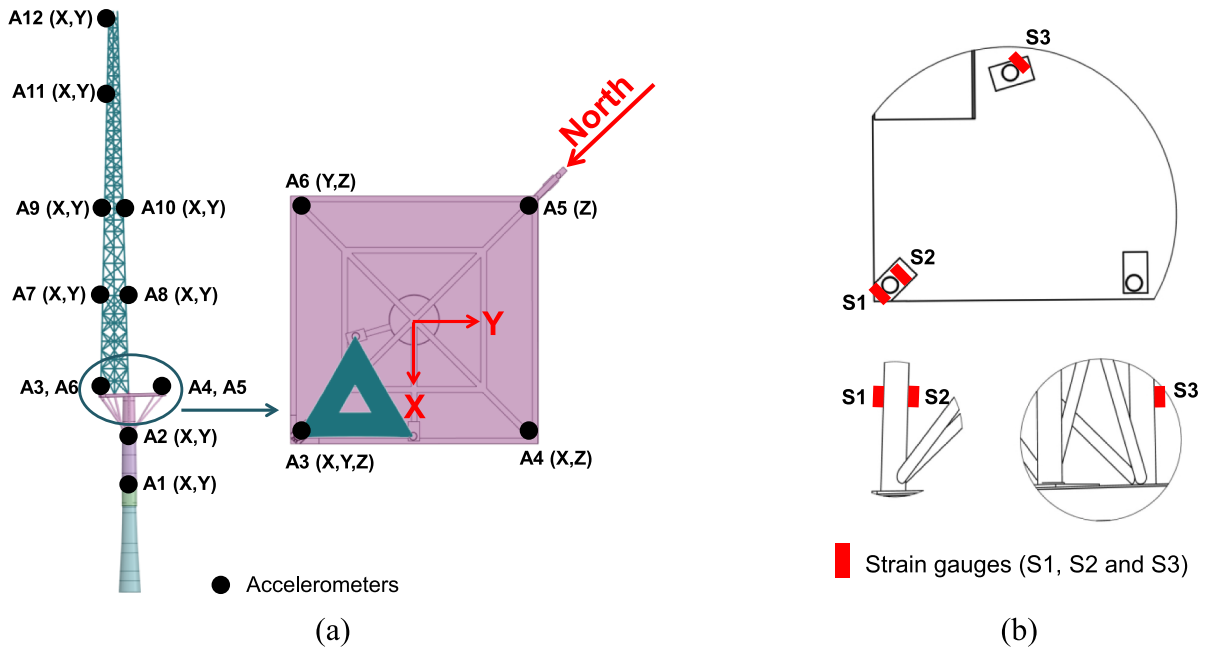


Fig. 2. Instrumentation details of FINO3: (a) layout of 12 accelerometers, and (b) 3 strain gauges.

in which f is the frequency, \bar{v} and σ_v denote the mean and standard deviation of wind speed. L denotes the integral length scale which is defined in the Det Norske Veritas code [65] and is equal to $5.67z$ when $z < 60$ m and 340.2 m when $z \geq 60$ m. Here z denotes the height above sea level. To simplify the input load, the wind profile along the height of the structure is assumed to follow the power law (Fig. 1(c)) based on the IEC 61400-1 code [66]:

$$v(z) = v_r(z/z_r)^{0.2} \quad (11)$$

Here v_r denotes the reference wind speed and represents the wind at the top of the structure, and $z_r = 103.75$ m is the total height of the structure above sea level. The wind load distribution along the height is related to the wind speed based on the following relationship [67]:

$$F(z) = 0.613v(z)^2 A(z) C_d \quad (12)$$

where $A(z)$ denotes the projected area of an object perpendicular to the wind direction. In this study, the areas of beam and truss elements in the FE model are projected perpendicular to the wind direction and are evenly distributed to the two end nodes of each element. C_d is drag coefficient and since FINO3 mainly consists of tube elements, C_d is assumed to be constant along the height. Substituting the power law profile in Eq. (11), the wind load vector $[F(z)]$, which consists of force at all nodes along the structural height, can be formulated as:

$$[F(z)] = [\varphi(z)] \times F_w \quad (13)$$

$$\varphi(z) = \frac{0.613(z/z_r)^{0.4} A(z)}{\sum_z 0.613(z/z_r)^{0.4} A(z)} \quad (14)$$

$$F_w = v_r^2 C_d \sum_z 0.613(z/z_r)^{0.4} A(z) \quad (15)$$

in which the summation operation sums over all nodes in the FE model above sea level. The vector $[\varphi(z)]$ can be treated as the wind load profile and F_w denotes the load amplitude. In this study, two independent wind time histories are simulated to represent the wind loads in X (v_r^x) and Y (v_r^y) directions based on the Kaimal spectrum with a mean $\bar{v} = 15$ m/s and a standard deviation $\sigma_v = 4$ m/s, as shown in Fig. 3. The corresponding wind load amplitudes in X and Y direction are denoted as F_w^x and F_w^y which can be evaluated based on Eq. (15) using reference wind speed v_r^x and v_r^y , respectively. The wind load profile $[\varphi(z)]$ is assumed to be the same in both directions. It is worth noting that the wind loads in X and Y directions can be correlated in practice, and the correlation relationship changes with the wind direction. However, by treating the wind loads in X and Y directions as independent and estimating them together, the wind direction and the changing correlation relationship can be ignored. Therefore, the proposed approach has a more universal nature for

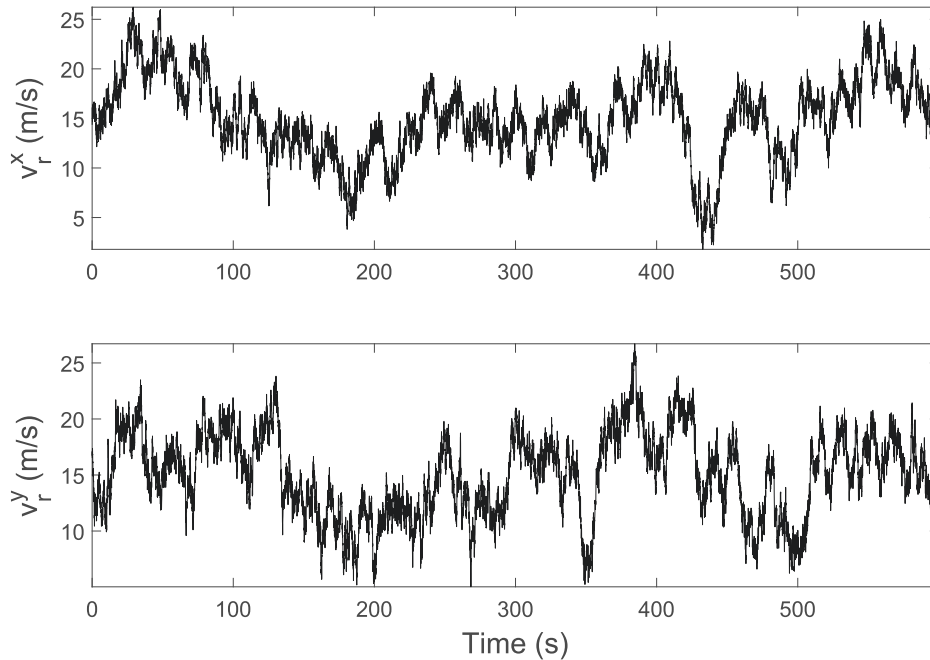


Fig. 3. Simulated wind speed time histories in X (v_r^x) and Y (v_r^y) directions.

wind load estimation but with the expense of more computational effort. The acceleration and strain measurements are simulated as the corresponding structural response collected by the accelerometers and strain gauges with a sampling frequency of 25 Hz. A total of 10 min response is simulated and polluted with 1% noise-signal-ratio (NSR) to account for the sensor noise.

4. Validation using numerically simulated data

4.1. Strain estimations from modal expansion and model updating

The modal parameters of the structure are identified using the simulated acceleration measurements. The data-driven stochastic subspace identification (SSI-DATA) method is employed to estimate the natural frequencies, mode shapes and damping ratios of the structure [68–70]. The stabilization diagram is shown in Fig. 4 together with the average power spectrum of all 24 channels of acceleration. The stabilization diagram plots the identified natural frequencies versus the system order used for model realization (the ordinate in Fig. 4 shows half of the system order). The natural frequencies that are repeated with increasing model order are deemed stable. The starred circles refer to stable modes and the horizontal green line denotes the final selected order of the state-space model for modal identification. The identified modal parameters are compared with the nominal/true values (from FE model) in Table 2. The modal assurance criterion (MAC) values are computed between identified and true mode shapes. Table 2 shows that the natural frequencies of the first 5 modes are identified with very high accuracy, except for mode 3 which could not be identified due to its low excitation by the simulated inputs. Small errors are observed for the identified natural frequencies of modes 6 and 7. All identified mode shapes have high accuracy with MAC values close to 1, except for mode 5. It is worth noting that modes 1 and 2 are the first bending modes in X and Y directions, and their natural frequencies are very closely spaced, as can be seen in Fig. 4. Modes 4 and 5 are the second bending modes in X and Y directions and their natural frequencies are also closely-spaced.

Model updating is performed to estimate the rotational stiffness k_R of the soil at the foundation using the identified natural frequencies and mode shapes of vibration modes 1 and 2. Higher modes are not used here because in real-world applications they cannot be identified with high accuracy, e.g., only the first two modes are accurately identified and correlated to the model in the experimental application in section 5. A global optimization strategy is employed in MATLAB [71] for model updating, and the optimal value of normalized k_R is 0.939, which has an error of 6.1%. The error is caused by the modal identification errors and the effect of regularization term in Eq. (4), since the initial value θ_0 here is assumed to be 0.7, which assigns penalty to values different from it.

For strain estimations using the modal expansion approach, predictions are divided into two frequency bands: dynamic (≥ 0.25 Hz) and quasi-static bands (< 0.25 Hz). The dynamic part of strains is estimated using displacement time histories which are numerically integrated twice from acceleration measurements. The displacements are then filtered through a high-pass finite impulse response (FIR) filter with a cutoff frequency of 0.25 Hz. The filtering process is to remove the low frequency contents of the integrated displacements which have high integration errors. It is worth noting that the cutoff frequency between dynamic and quasi-static bands is usually chosen in the range of 0.15 to 0.25 Hz, and no significant difference is found for values within this range [50]. The mode shape

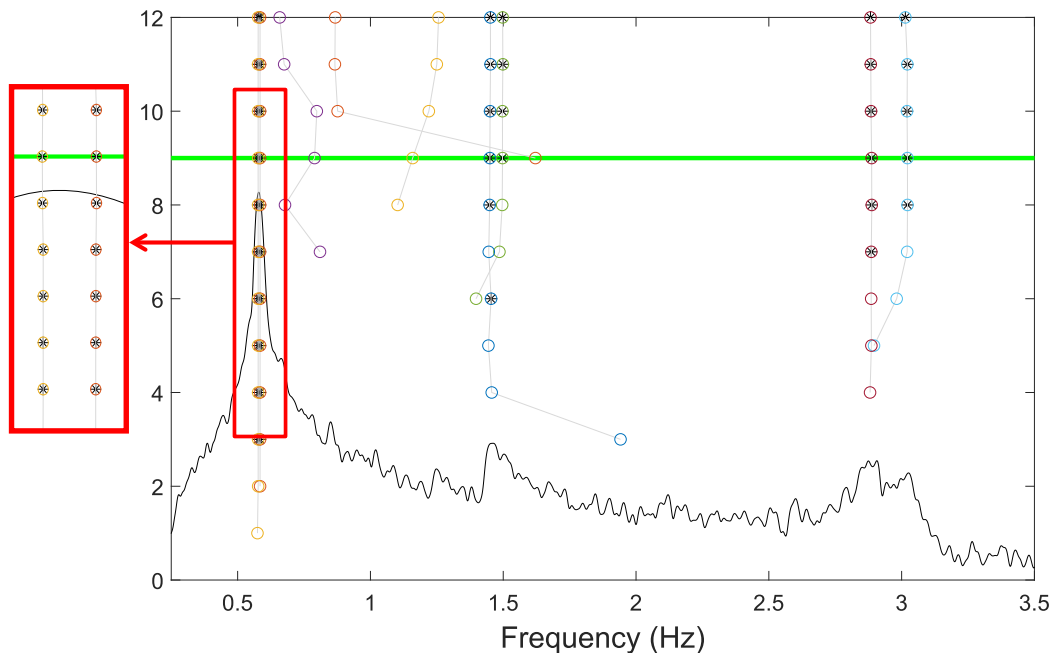


Fig. 4. Frequency stabilization diagram using simulated acceleration measurements.

Table 2

Comparison of identified natural frequencies and mode shapes with the nominal/true values.

Mode	Natural frequency (Hz)		Mode shape (MAC)
	True	SSI-DATA	
1	0.58	0.58	0.99
2	0.59	0.59	0.99
3	1.27	–	–
4	1.46	1.45	1.00
5	1.51	1.50	0.86
6	3.03	2.89	1.00
7	3.18	3.02	1.00

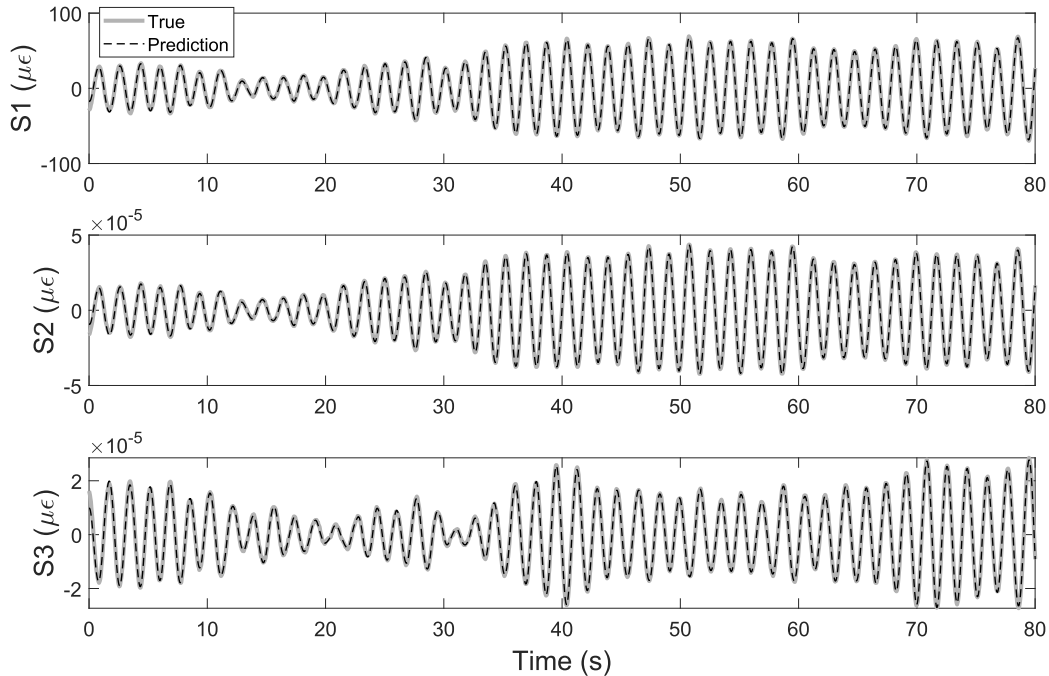
matrix $\Phi_u(\theta^{opt})$ in Eq. (8) only includes the first two modes, which provided dominant contribution to the structural response. The modal contribution $q(t)$ is computed using all 24 channels of displacements, and then strain time histories at dynamic band are predicted using Eq. (9) and are compared with their true values (also filtered ≥ 0.25 Hz) in Fig. 5. Excellent agreement is observed between strain predictions and their true values. For the quasi-static band, strain measurements of S1 and S3 are used to estimate the modal contributions of the first two modes. S1 and S3 data are first filtered below 0.25 Hz using a complimentary low-pass FIR filter and then used for prediction of S2. The quasi-static strain predictions and their true strain time histories are compared in Fig. 6, which shows that the prediction of S2 has very high accuracy. Note that since S1 and S3 are used for computing modal contribution, their quasi-static predictions have zero error because the pseudo-inverse solution is determined (two equation with two unknowns). The total strain predictions are shown in Fig. 7 by simply adding the dynamic and quasi-static predictions. The prediction accuracy is evaluated using relative root-mean-square error (RRMSE) which is defined as:

$$RRMSE(a) = \frac{RMS(a - a^{true})}{RMS(a^{true})} \times 100\% \quad (12)$$

where a and a^{true} denote the predicted and true response time histories, respectively. The RRMSE for S1, S2 and S3 at dynamic, quasi-static, and full bands are reported in Table 3. Overall, the RRMSE of strain predictions are very small.

4.2. Joint Parameter-Input estimation from UKF

The proposed window-based UKF method for joint parameter-input estimation in Section 2.1 is implemented here to estimate the rotational stiffness k_R and the wind loads in X (F_w^x) and Y (F_w^y) directions. Zero initial conditions (ICs) are assumed for the structural response of the FE model, while in reality, the structure is continuously vibrating and therefore has non-zero ICs. To consider the effects

**Fig. 5.** Strain time history predictions at dynamic band.

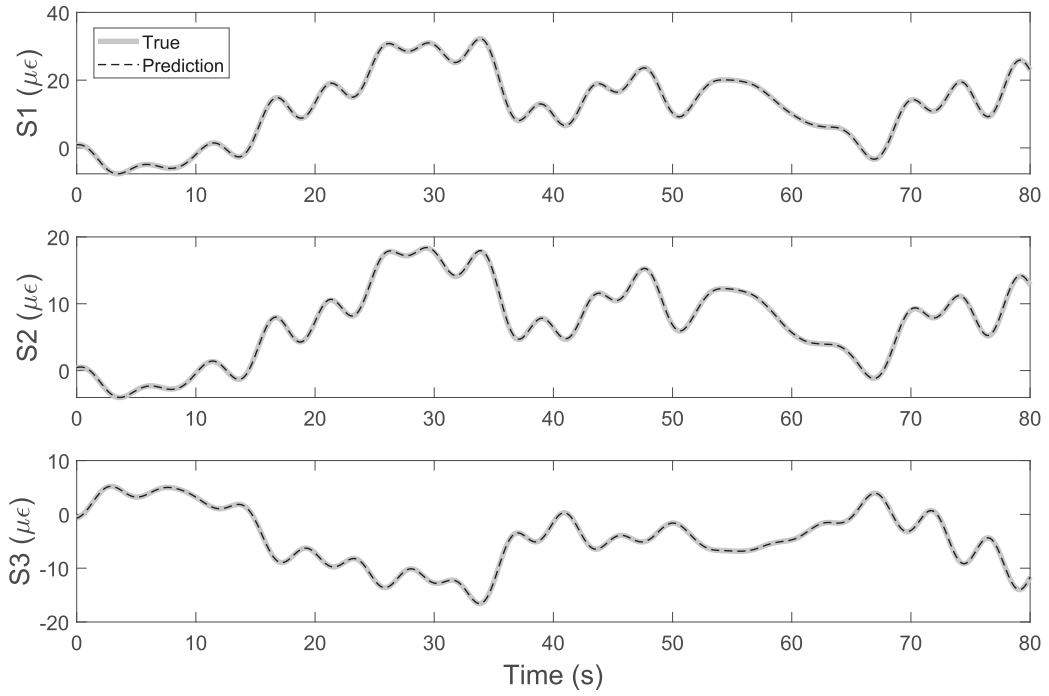


Fig. 6. Strain time history predictions at quasi-static band.

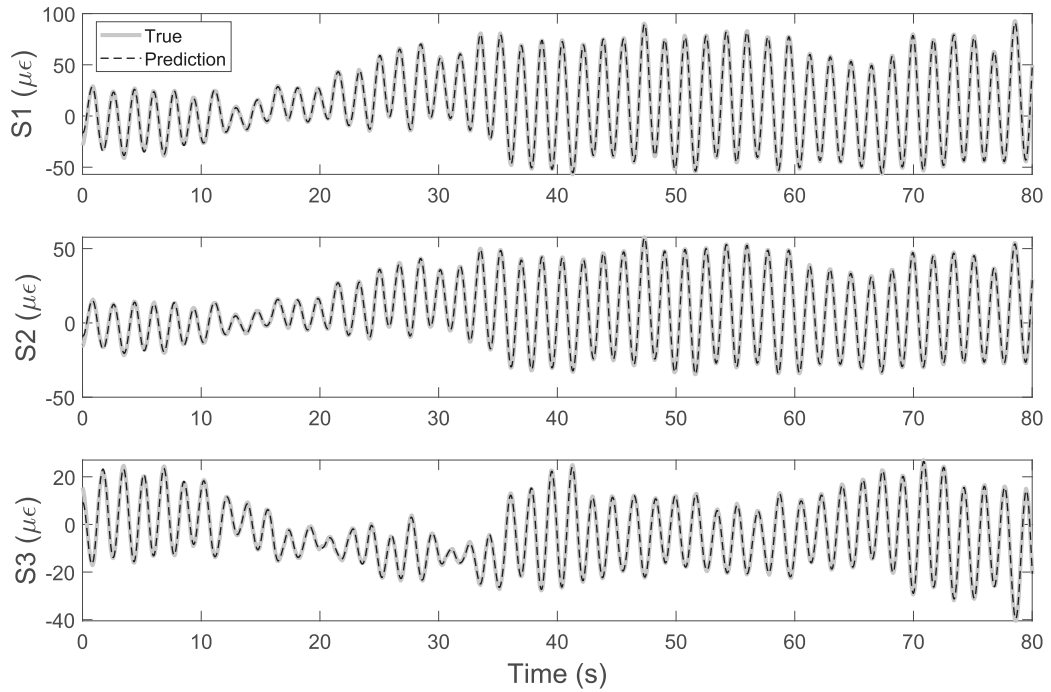


Fig. 7. Total strain time history predictions combining dynamic and quasi-static bands.

of ICs in this numerical study, the UKF is performed using the simulated structural response starting from the fourth minute, i.e., the structure is assumed to reach a steady state after three minutes and the first three minutes of response are discarded. The joint parameter-input estimation is first implemented using the dynamic part of acceleration measurements (≥ 0.25 Hz), because the

Table 3
RRMSE (%) of strain predictions and input estimations.

	Modal Expansion			UKF		
	Dynamic	Quasi-static	Full band	Dynamic	Quasi-static	Full band
S1	2.6	0	2.4	3.6	0.04	2.1
S2	2.5	1.0	2.3	4.0	0.5	2.2
S3	2.9	0	2.5	2.6	0.4	2.1
F_w^x	–	–	–	9.2	0.8	1.3
F_w^y	–	–	–	13.7	1.0	2.2

parameter k_R cannot be determined using quasi-static measurements as the structure is statically determined. The input loads at quasi-static band are then estimated using strain measurements (<0.25 Hz). The initial value of normalized rotational stiffness θ_0 is set to be 0.7 (the same as the modal expansion approach), the initial variance of model parameter is $P_0^{\theta} = (0.3\theta_0)^2$, and the initial variance of input loads for F_w^x and F_w^y are assumed to be the same and defined as $P_0^f = \text{diag}(0.5\mathbf{1}_{1 \times L})^2$. For the joint estimation process, the input loads F_w^x and F_w^y are normalized by 3 kN for the dynamic band, and 20 kN for the quasi-static band. The normalization is to ensure the model parameter and input values fall in similar range and avoid numerical issues. The process noise variance of model parameter is set to be $Q^{\theta} = (10^{-3}\theta_0)^2$, and process noise variance for both input loads are set to be the same and equal to $Q^f = \text{diag}(0.01\mathbf{1}_{1 \times L})^2$. The measurement noise variance is defined as $R = \text{diag}([R_1 \mathbf{1}_{1 \times L} \cdots R_m \mathbf{1}_{1 \times L}])$ in which R_i is based on the polluted noise of 1% NSR and is equal to $R_i = \text{diag}(0.01\text{RMS}(\mathbf{y}^{\text{true}}))^2$ in which \mathbf{y}^{true} denotes the simulated true response of channel i . The window length L is set to 100 time steps (i.e., 4 s for sampling frequency of 25 Hz) and the overlap between windows is equal to 50. A total of 60 s of input loads are estimated, which contains 29 windows. The convergence criterion ε is set to 0.03. In this study, the convergence criterion was easily satisfied at every time window. However, limiting the maximum number of iterations might be needed in applications when the criterion cannot be satisfied, or the convergence takes too long. The parameter evolution history in all iterations and all windows is shown in Fig. 8. The parameter estimation converges to the true value after 10 iterations, and then generally stays stable. The final estimated value is 1.008 which is more accurate than the result of model updating (0.939). The estimated input loads at the dynamic band are shown in Fig. 9. Note that the estimations are separated into two subfigures for better visualization as different scaling are used in Fig. 9(a and b). Large estimation errors are observed in the first few seconds of the input time histories, which is caused by the effect of at rest ICs in model response. Approximately 10 s of input estimations are affected by the ICs and can be simply discarded. The remaining (past 10 s) parts of estimations have very good accuracy as shown in Fig. 9(b). The acceleration predictions using the estimated model parameter and input loads are shown in Fig. 10 for accelerometer A12 in X and Y directions. It is interesting to observe that the predictions match their true response very well even for the initial part of the signal, indicating that the estimated bias in input loads has successfully compensated the effects of wrong ICs assumption.

For the estimation of quasi-static input loads, since the model parameter is already estimated using the dynamic response, it is excluded in the state vector ψ which now only includes input loads. Note that unlike the dynamic band, only one window is used here, i.e., the total length of the quasi-static input loads is included in the state vector. Another difference is that the proposed UKF algorithm in Table 1 will not include iterations in this case, which means the algorithm runs from step (1.1) to (2.6) only once without the convergence test. The same algorithm used for the dynamic band can still be used here, simply by excluding model parameter, choosing window length equal to the total length of signal, and setting a large convergence criterion. All these modifications for the quasi-static band are made and verified based on the authors' experience and trial-and-error process and have worked well in studied applications. The estimated quasi-static part of the inputs is shown in Fig. 11, which is also separated into two subplots for better visualization. It is seen that the initial and tail part of estimation has large variability, while the middle part shows smaller rippling effects. The cause of the estimation errors in the initial part is the ICs assumption, while it is due to the low sensitivity of input estimation for the tail part. The rippling effects can be easily removed by a low-pass filter since the quasi-static loads are not expected

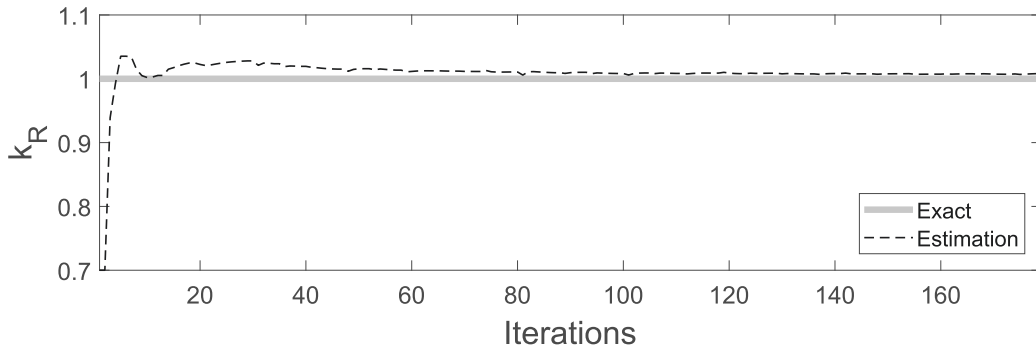


Fig. 8. Parameter evolution history of all iterations.

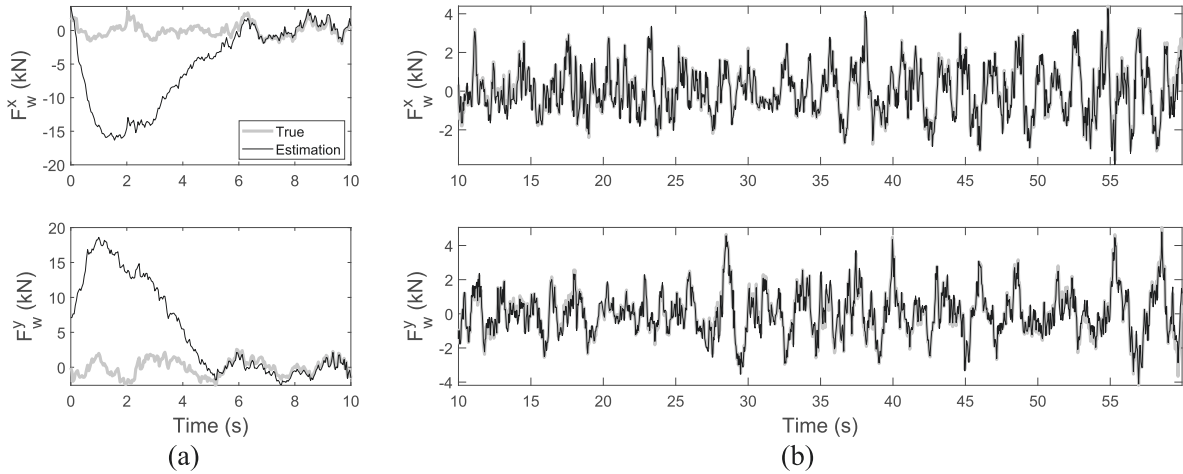


Fig. 9. Estimated input loads at dynamic band: (a) 0–10 s and (b) 10–60 s.

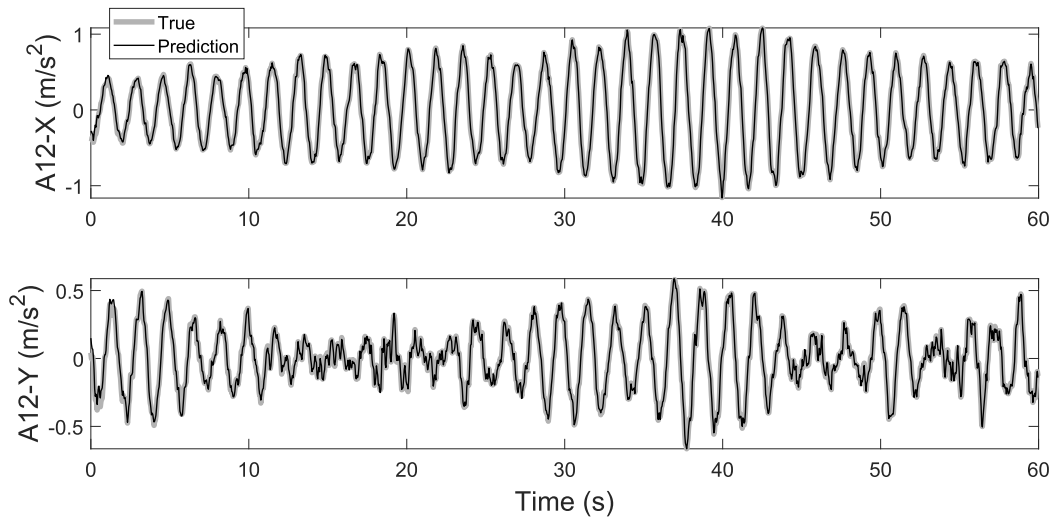


Fig. 10. Acceleration predictions using estimated model parameter and dynamic input loads.

to contain higher frequency content. An FIR filter of order of 100 and a cutoff frequency at 0.5 Hz is used here. The filtered input estimations are shown in Fig. 11(c). The filtered estimations match the true values very well, except for the initial few seconds which is affected by the ICs. The strain predictions using the unfiltered estimated quasi-static inputs are shown in Fig. 12. Although the input estimations have large variability and rippling effects, strain predictions are considerably accurate. To further study the cause of the higher frequency content (rippling), the strain predictions using the filtered input estimations (Fig. 11(c)) and their Fourier amplitude spectrum (FAS) are plotted in Fig. 13. It is seen that, although the filtered input estimation is very accurate, the strain predictions show similar rippling phenomenon with frequency of 0.59 Hz which correspond to the natural frequencies of the first two modes in Table 2. Therefore, the rippling effect in the estimated quasi-static inputs is compensating the modal contribution of the first two modes in the model response. Note that this rippling phenomenon cannot be removed by using more windows or more iterations.

The total estimated input loads can be obtained by the addition of dynamic and quasi-static estimations, as shown in Fig. 14. Note the filtered quasi-static input estimations (Fig. 11(c)) are used here and the first 10 s are excluded. The total input estimations are shown to have very high accuracy. For the total strain predictions, the original/unfiltered quasi-static input estimations are used here. The strain predictions, as shown in Fig. 15, agree well with the true values, except for the initial part due to the ICs. The RRMSE of strain predictions and input estimations are reported in Table 3. The RRMSE are evaluated for signals between 10 s and 60 s. It is seen that the traditional modal expansion approach and UKF method provide comparable accuracy for strain predictions. The advantage of UKF is to provide input estimations which are not available from modal expansion approach. It is worth noting that the total input estimations in Fig. 14 (with filtered quasi-static part) can also be used for strain predictions, and results are similar but slightly less accurate (compared to using unfiltered quasi-static estimations) with RRMSE of 5.4%, 5.8% and 5.0% for S1, S2 and S3, respectively.

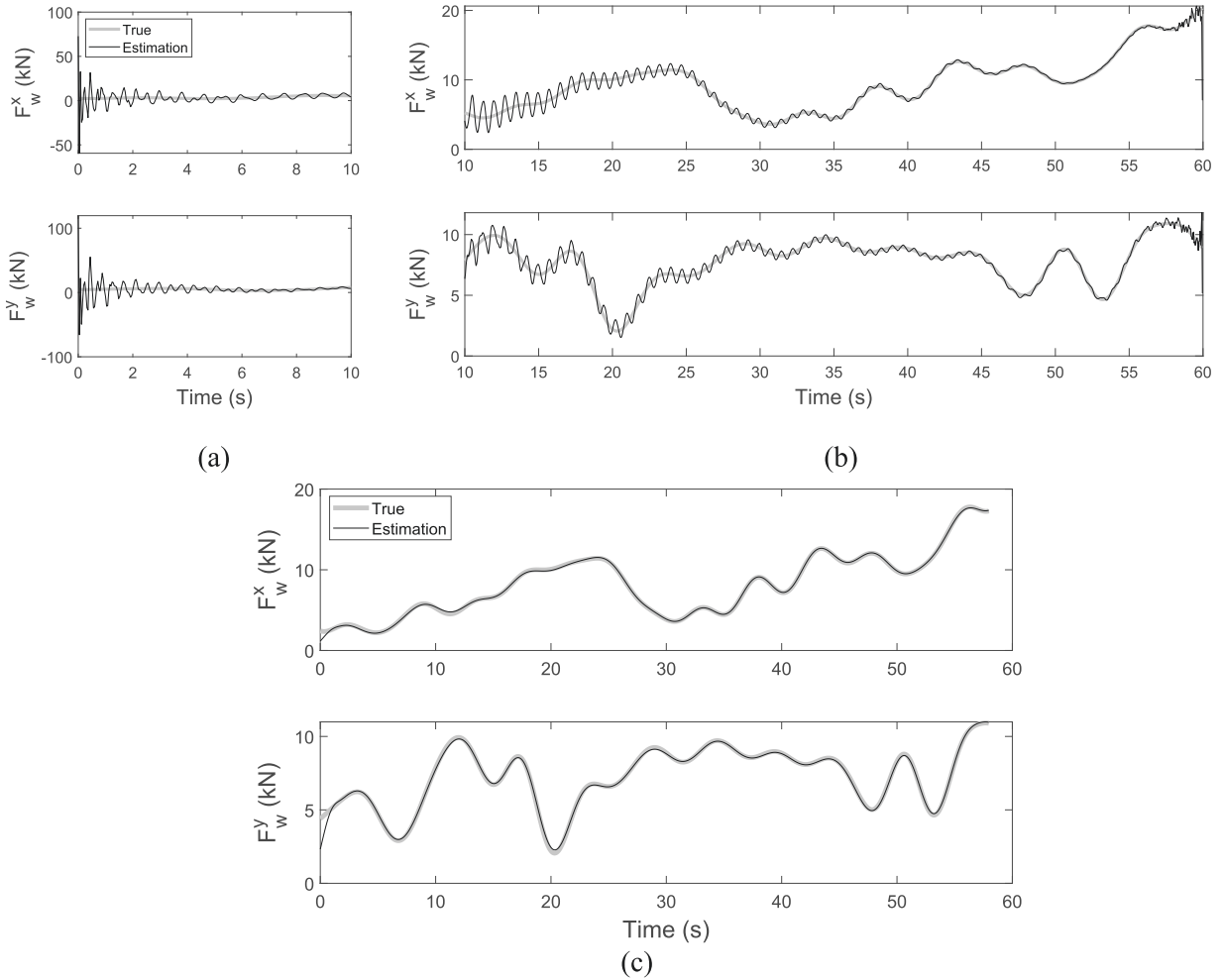


Fig. 11. Estimated input loads at quasi-static band: original estimations between 0 and 10 s (a) and 10–60 s (b), and filtered estimations (c).

5. Validation using *in-situ* measured data

5.1. Modal expansion and model updating

The measurements of FINO3 structure used in this study were discussed in Section 3. The SSI-DATA method is applied to identify the modal properties of FINO3 using acceleration measurements. Four significant modes are identified with natural frequencies of 0.419 Hz, 0.427 Hz, 0.985 Hz and 0.993 Hz. Modes 1 and 2 are the first bending modes in X and Y directions, respectively, with closely spaced natural frequencies. Modes 3 and 4 are the second bending modes in X and Y directions and are also closely spaced. The mode pairing between the FE model and the identified modes are shown in Fig. 16 using the MAC values between mode shapes. It is seen that the identified modes 1 and 2 corresponds to the first two modes of the FE model with high MAC values, while the identified modes 3 and 4 corresponds to the modes 5 and 4 of the model with relatively lower MAC. Mode 3 of the model is not identified from the data, similar to the simulation case. Since only the first two modes of FINO3 are identified with relatively high accuracy, the model updating process is performed using only these two modes, as it was done in the previous section. The initial value of the rotational stiffness k_R is assumed to be 25 GN/rad with the normalized parameter $\theta_0 = 1$. A global optimization is performed using MATLAB and the optimal value of updating parameters is found as 0.186, which is significantly smaller than its initial value. This is expected since the natural frequencies of the initial FE model are considerably higher than the identified values (shown in Table 4), which means the initial model is much stiffer than the actual structure. Thus, the reduction in soil stiffness compensates for such discrepancy between initial model and measured data. The modal parameters of the model before and after model updating are compared with the identified values in Table 4. It is found that the natural frequencies of the FE model have been drastically improved and are very close to their identified counterparts after model updating. However, the mode shapes already had excellent agreement with measurements and the MAC values generally stay the same after updating.

The same procedure of the modal expansion approach presented in the numerical case is applied here for strain time history

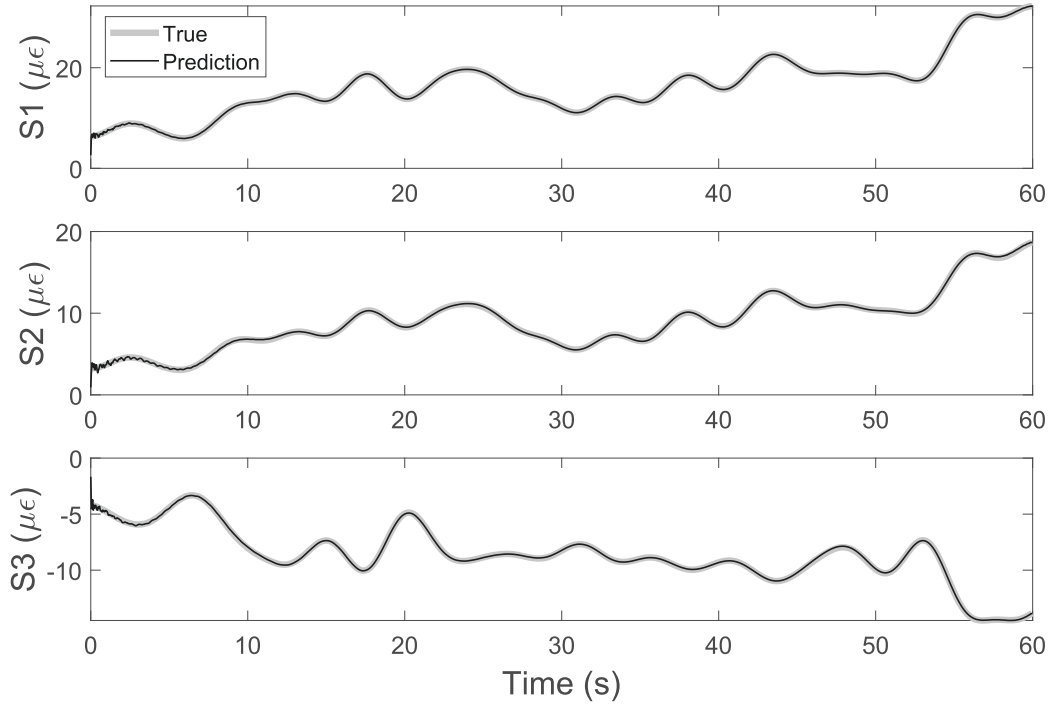


Fig. 12. Strain predictions using estimated quasi-static input loads.

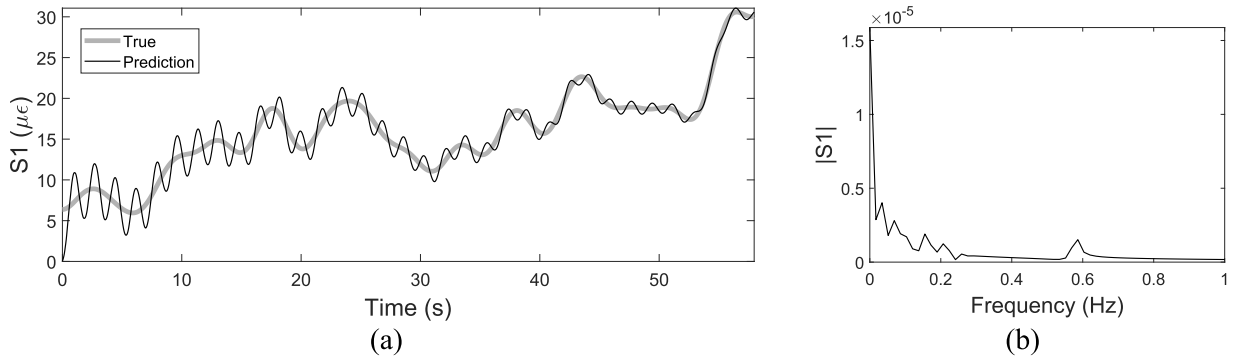


Fig. 13. Strain prediction using filtered input estimations at quasi-static band (a) and its FAS (b).

prediction, i.e., strain predictions are divided into dynamic and quasi-static bands. The dynamic part is estimated using displacements integrated from acceleration data and the quasi-static part is computed using strain data (S1 and S3). Similar to the previous case, only the contributions of the first two modes are used here for modal expansion. The dynamic, quasi-static, and total strain predictions are shown in Fig. 17, Fig. 18 and Fig. 19, respectively. It can be observed that the predicted dynamic part of strain time history at S1 agrees with measurements very well, but the amplitude of S2 is underestimated, and S3 prediction has the worst accuracy due to the large measurement noise at this location. For the quasi-static band, S1 and S3 predictions match the measurements exactly because they are used for estimation and the pseudo-inverse solution is exact for a determined problem. The prediction of S2 at quasi-static band shows some errors partly due to the large noise in S3 data. The RRMSE of predictions at different bands are summarized in Table 5. The best prediction is obtained for S1, and the worst result is observed for S3. The RRMSE values seem relatively large, especially for S3, which is due to the high sensor noise and some modeling errors in the FE model. Overall, the predictions are still acceptable considering this is a real-world case and one of the strain gauges provide very noisy data.

5.2. UKF results

Application of the proposed windowed UKF for joint parameter-input estimation is implemented here using the acceleration and

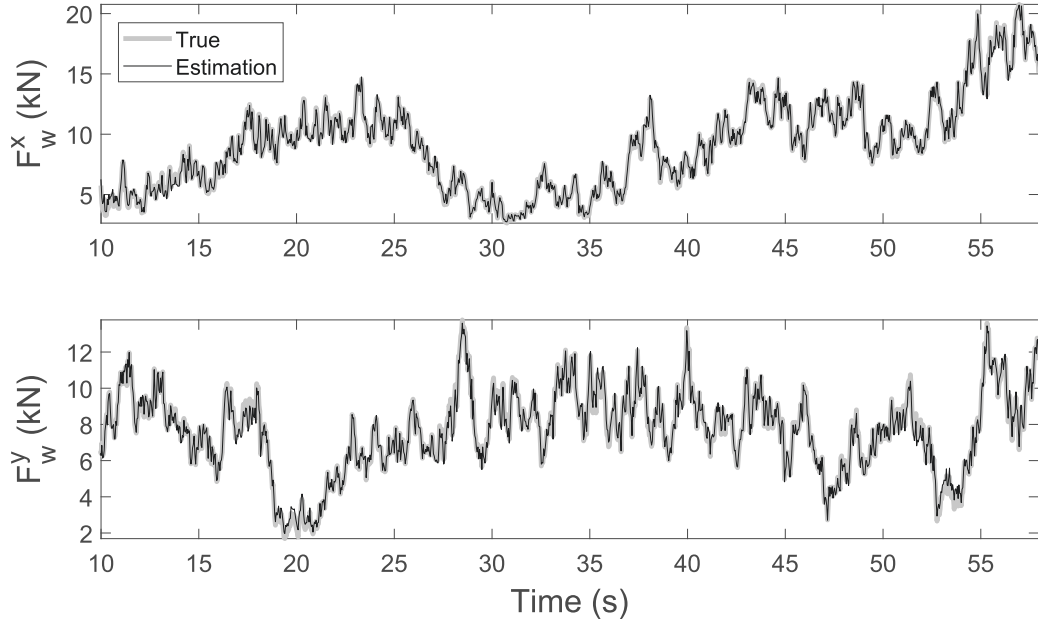


Fig. 14. Estimated input loads combining dynamic and quasi-static bands.

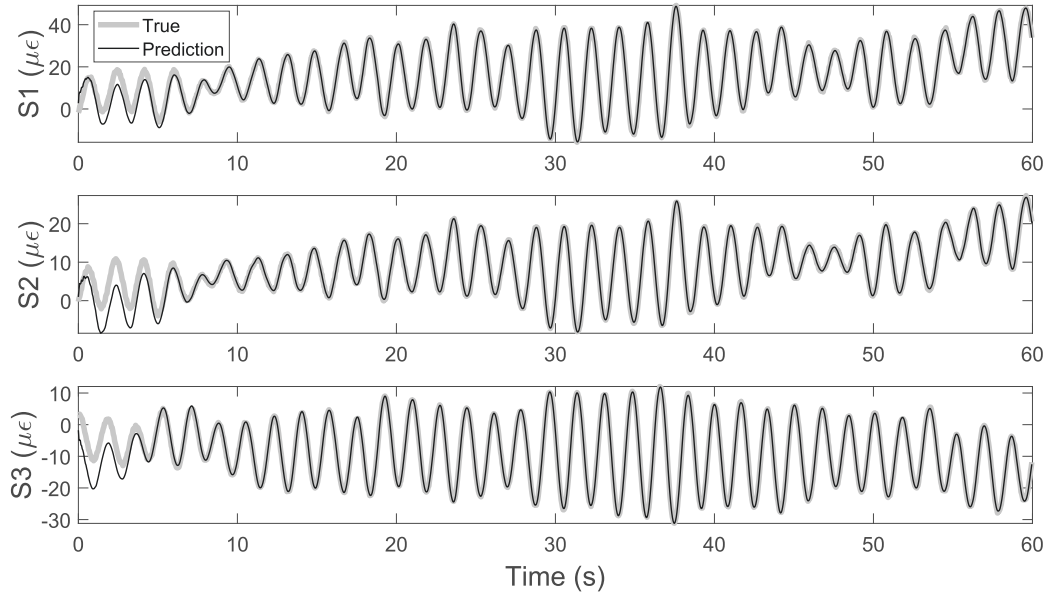


Fig. 15. Total strain predictions using the total estimated input loads.

strain measurements of FINO3. The measurement noise covariance \mathbf{R} is assumed considering 5% NSR, which is chosen to be relatively large to compensate for the modeling errors and measurement noise. Similar to the modal expansion approach, the initial value of updating parameter θ_0 is normalized to 1. The input loads F_w^x and F_w^y are normalized by 3 kN for the dynamic band, and 10 kN for quasi-static band. The window length is set as 100 (4 s long) with an overlap of 25 (25%). Other settings are the same as the simulation case, except the convergence criterion is set as 0.05. A total of 58 s of input loads are estimated. The parameter estimation is shown in Fig. 20 as a function of iterations. The stiffness k_R converges within three iterations and then stays generally stable. The estimated model parameter is equal to 0.181, which is very close to the previous result of model updating ($\theta^{opt} = 0.186$). The estimated input loads at the dynamic band are shown in Fig. 21 and the acceleration predictions are shown in Fig. 22. The acceleration predictions generally agree with the measurements but cannot capture their high frequency contents. The quasi-static part of input loads is estimated

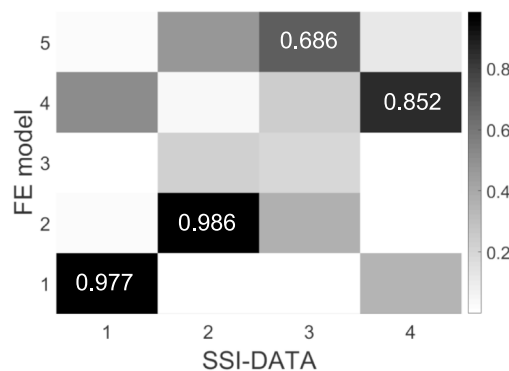


Fig. 16. Mode pairing using MAC between identified and initial FE model-predicted mode shapes.

Table 4

Comparison of modal parameters of model with identified values before and after model updating.

Mode	Frequency (Hz)			Mode shape (MAC)	
	Identified	Initial	Updated	Initial	Updated
1	0.419	0.578	0.424	0.977	0.977
2	0.427	0.587	0.427	0.986	0.969

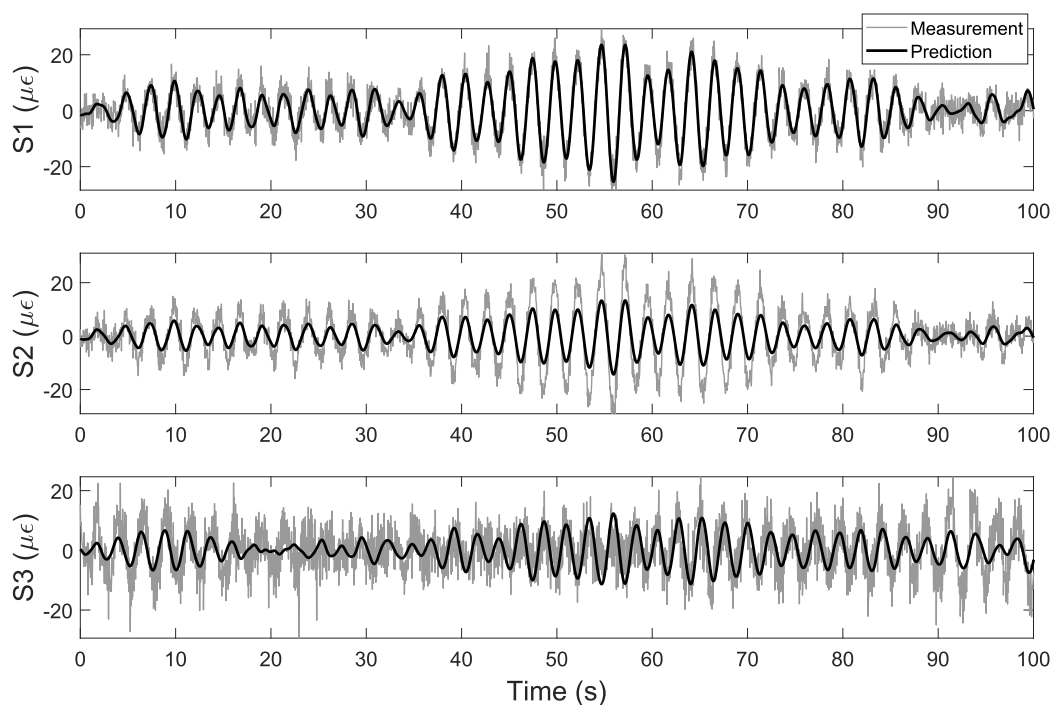


Fig. 17. Strain predictions of FINO3 at dynamic band.

following the same procedure in the simulation case. The input estimations at quasi-static band are shown in Fig. 23. It is found that the input estimations have evident variability at the beginning part of the signal which is caused by the ICs, and the similar rippling effect observed in the simulation study is also present here but with smaller amplitude, probably due to the larger noise variance R used here. The quasi-static input estimations can be improved by using the same filtering strategy as in the simulation study, and the filtered results are shown in Fig. 23. The corresponding quasi-static strain predictions are shown in Fig. 24. Accurate predictions are obtained

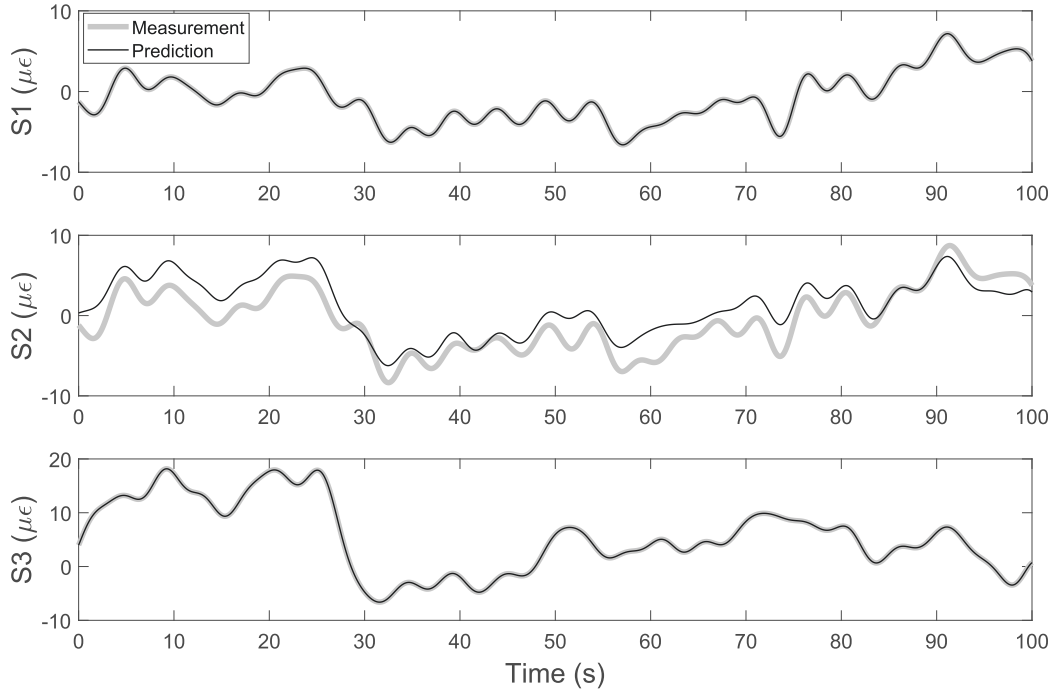


Fig. 18. Strain predictions of FINO3 at quasi-static band.

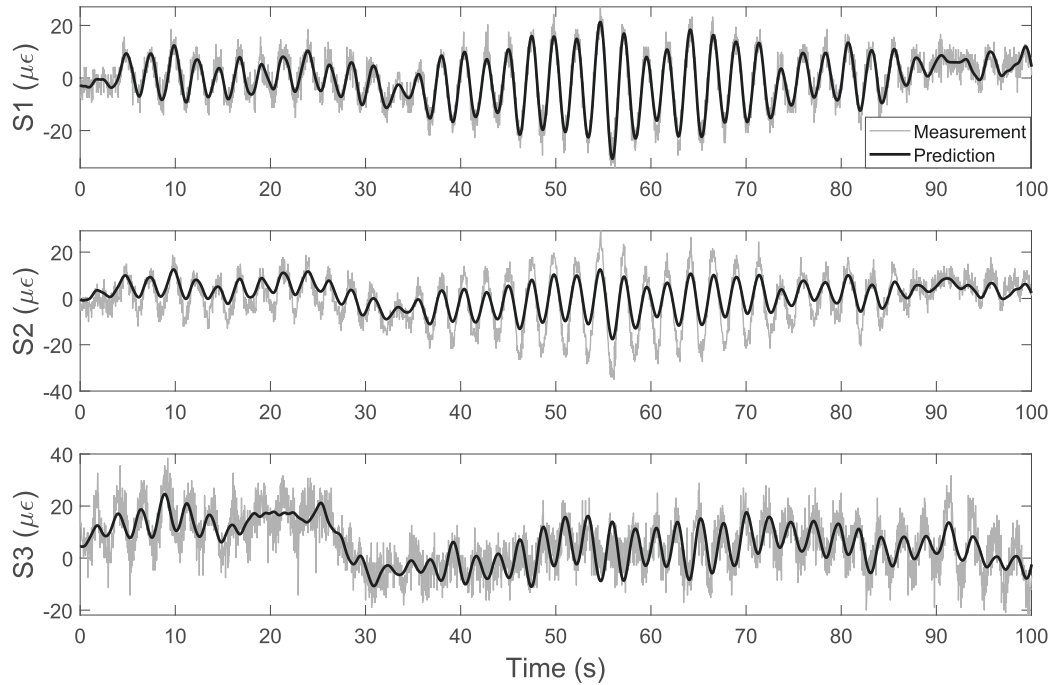


Fig. 19. Total strain predictions of FINO3.

for S1 and S3 because they are used for input estimation, while S2 prediction shows noticeable errors. The total input estimations are obtained by adding up the dynamic and filtered quasi-static bands which are shown in Fig. 25. It is observed that the input estimations in X (F_w^x) and Y (F_w^y) directions are roughly symmetric in time, which means they are highly correlated. This is expected since the wind

Table 5
RRMSE (%) of strain predictions of FINO3.

	Modal Expansion			UKF		
	Dynamic	Quasi-static	Full band	Dynamic	Quasi-static	Full band
S1	48.0	0	45.3	41.1	0.9	38.5
S2	59.3	51.3	58.3	60.6	49.8	58.9
S3	90.8	0	71.5	96.2	3.5	60.7

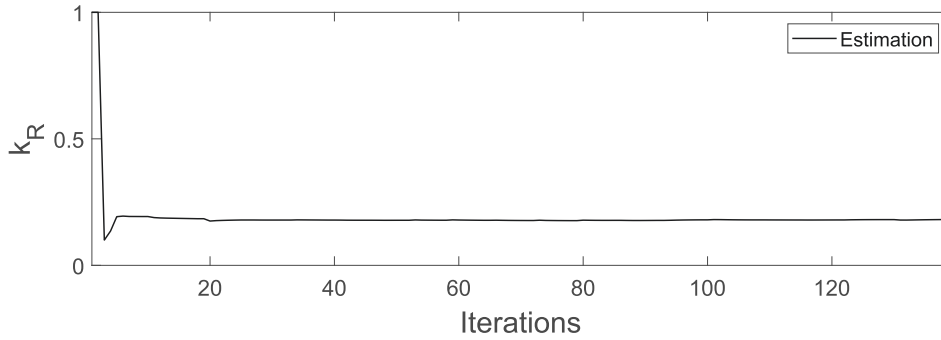


Fig. 20. Parameter evolution history using acceleration measurements of FINO3.

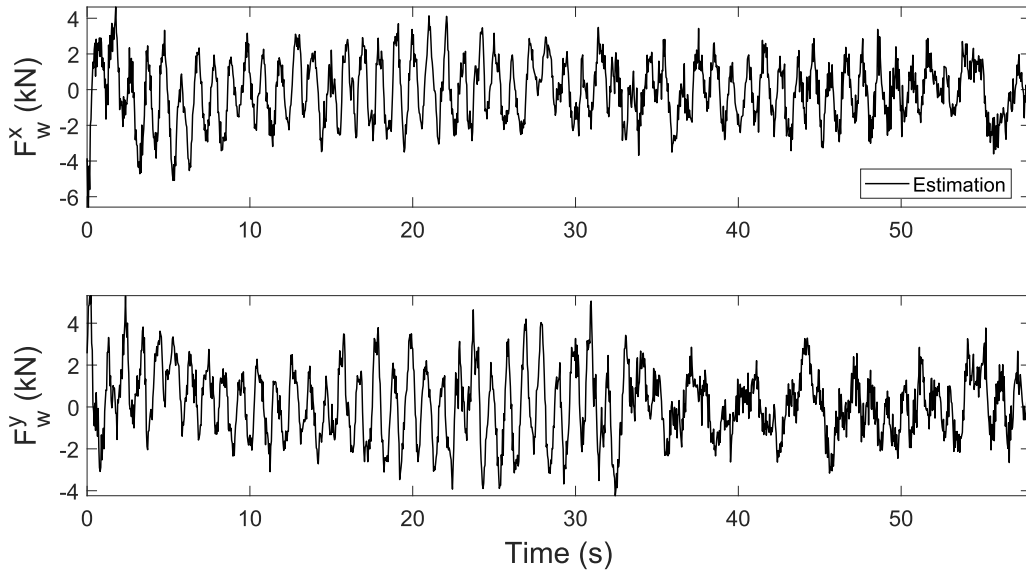


Fig. 21. Input estimations at dynamic band of FINO3.

loads excite the structure in one direction and the force is distributed into X and Y directions. The adopted strategy of estimating forces in X and Y independently increases the flexibility of the algorithm with the expense of more computational efforts. The total strain predictions are shown in Fig. 26 where the unfiltered quasi-static estimations are used here to obtain the total input loads. It is worth noting that the filtered quasi-static estimations can also be used here which provides almost the same accuracy as shown in Fig. 26. The S1 and S2 predictions generally agree with measurements well with slightly overestimated and underestimated amplitudes, respectively. The S3 prediction has the largest error due to the larger measurement noise of this channel. The RRMSE of strain predictions at different bands are reported in Table 5 where the first 5 s of signals are excluded to remove the effect of ICs. It is seen that the UKF algorithm provides more accurate strain predictions than the modal expansion method, which is probably due to the benefit of input estimation which partly compensates for modeling errors, while the modal expansion approach highly depends on the modeling accuracy.

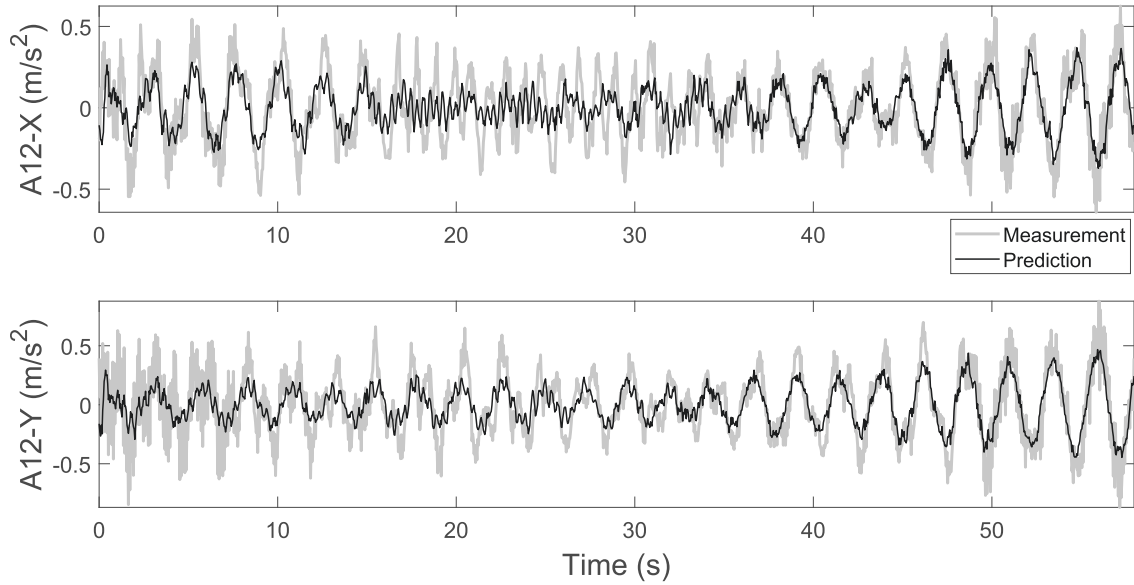


Fig. 22. Acceleration predictions (A12-X and Y) using estimated dynamic input loads.

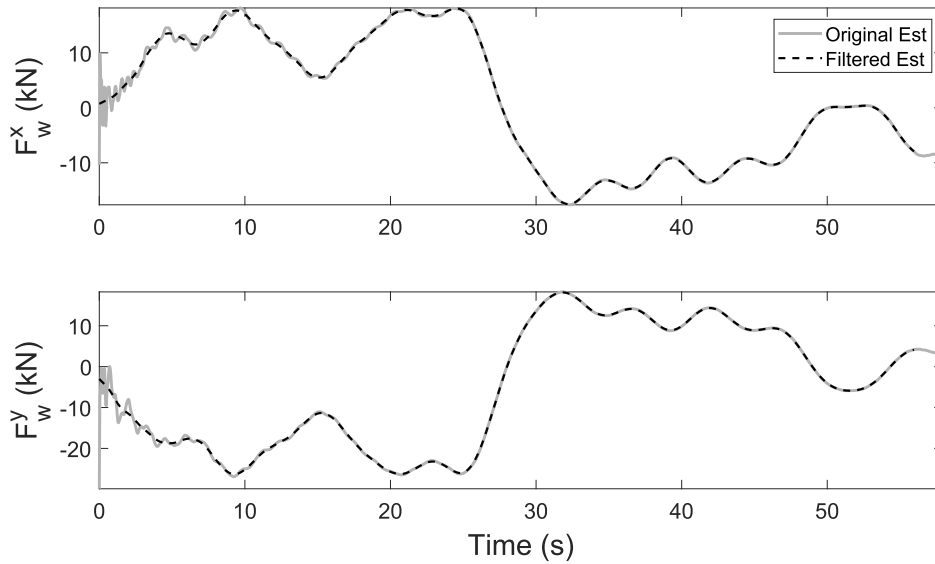


Fig. 23. Input estimations at quasi-static band using measurements of S1 and S3.

6. Summary and conclusions

This paper presents a recursive Bayesian inference framework for joint parameter-input estimation and its application for strain predictions of the offshore platform FINO3 using sparse output-only measurements. The UKF algorithm is implemented to jointly estimate the rotational stiffness at the foundation and independent input loads in X and Y directions. The input loads are estimated at overlapping time windows by augmenting the state vector with model parameters of interest and input loads at each window. The input loads are identified separately at two bands: dynamic and quasi-static. The dynamic parts of loads and model parameters are estimated using acceleration data, and the quasi-static loads are estimated using strain measurements. A traditional modal expansion approach combined with model updating is also performed for strain predictions and compared with the UKF method. The proposed approach is first evaluated numerically using an FE model of FINO3. Accurate model parameter and input load time histories are obtained, and strain predictions have high accuracy, similar to the modal expansion approach. Then these two methods are further demonstrated using the actual measurements of FINO3, and in this case, the UKF provides more accurate strain predictions than the

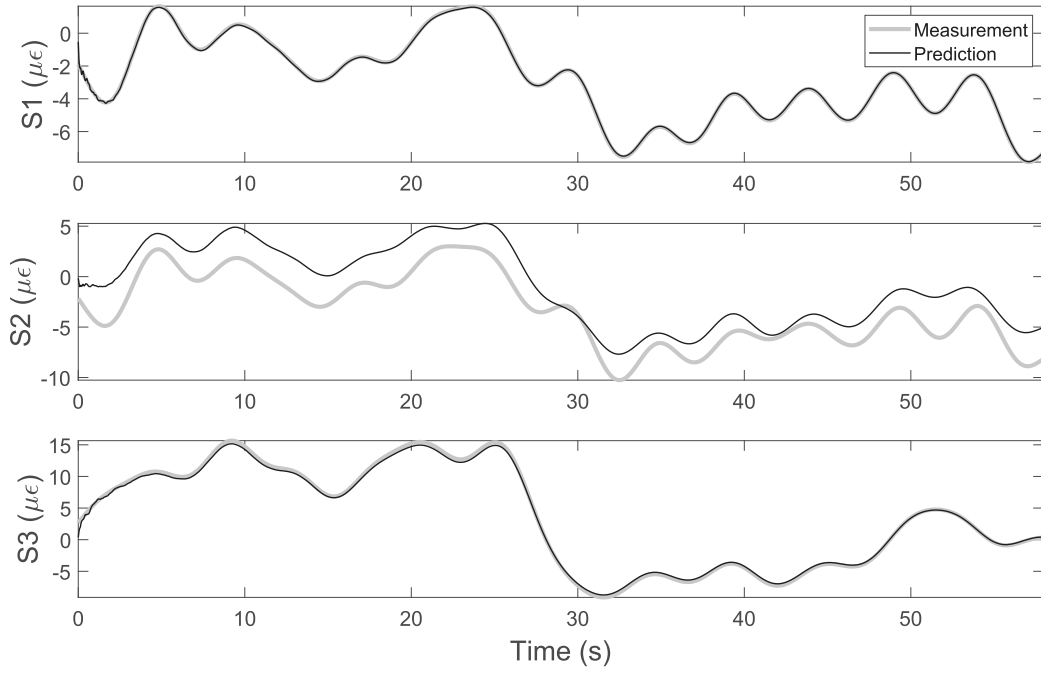


Fig. 24. Strain predictions using estimated quasi-static input loads.

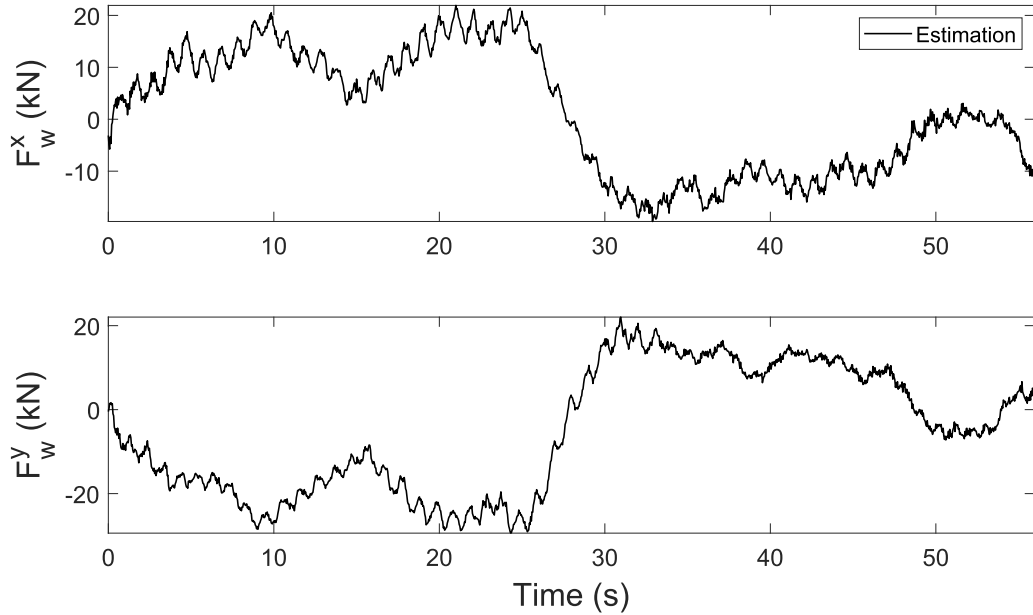


Fig. 25. Total input loads estimations for FINO3.

modal expansion approach. The rotational stiffness estimations using the two methods are highly consistent. In this study, high-pass filtering of acceleration (≥ 0.25 Hz) and low-pass filtering of strain measurements (< 0.25 Hz) are required as data pre-treatment, in addition to the numerical integration of acceleration data to compute displacements in the modal expansion approach. The following conclusions are made from the comparison of the two implemented methods for virtual sensing.

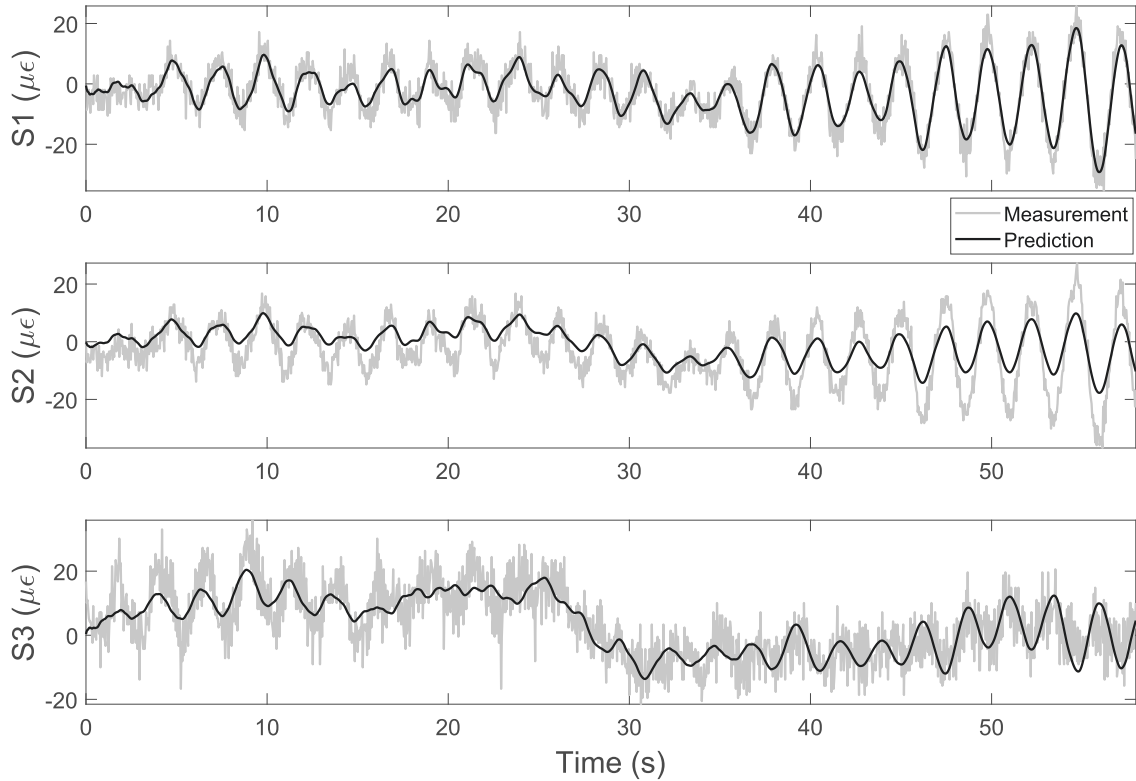


Fig. 26. Total strain predictions using estimated inputs for FINO3.

- (I) The main benefit of the proposed windowed UKF method is its capability to estimate the input loads which are not readily available from the modal expansion approach. The estimated inputs can be useful for the purpose of design, assessment and monitoring of similar structures.
- (II) When modeling error is small and measurements are clean as in the numerical study, parameter estimation is accurate using both UKF and modal expansion methods, with slightly higher accuracy observed for UKF. The input estimations from UKF are very accurate and only the beginning part of the input signals is affected by ICs. Strain predictions have comparable high accuracy using both methods.
- (III) In the presence of large modeling error and measurements noise, the UKF provides more accurate strain predictions than modal expansion, probably because the estimation of input loads partly compensates for modeling error, while the modal expansion approach is highly sensitive to modeling accuracy.
- (IV) Similar to other types of KF methods, performance of the proposed UKF approach is subject to filter parameters (e.g., ψ_0 , P_0 , Q , R). Although there is no one parameter setting that is optimal for all applications, some general rules can be followed to choose and adjust these parameters for specific application. For example, the initial values of model parameters should be selected based on the design information when available. The initial covariance of model parameters is inversely proportional to the uncertainty of initial values, i.e., a relatively large covariance should be used if the initial values are highly uncertain. The process noise covariance Q should be selected relatively small but not zero, to provide enough uncertainty/energy to promote the filter move to the high probability region of the posterior parameter space, but not to introduce too much variability to cause divergence. Based on previous studies, the measurement noise R should consider the effects of both sensor noise and modeling errors [38,72]. Therefore, a relatively large R is preferred if significant modeling errors are observed. Alternatively, adaptive KF can be applied which updates R along the estimation of state vector [39,72]. The setting values used in this paper are based on authors' experience and can be used as the first-trial setting for applications to similar dynamic systems.
- (V) The UKF method for joint parameter-input estimation is computationally expensive, with most of the computation effort coming from evaluating the SP (Step (1.3) in Table 1). This process can be sped up by adopting a parallel computing strategy as SP computations are independent. On the other hand, the modal expansion approach is computationally efficient and strain predictions can be completed within seconds after the model is calibrated.
- (VI) The joint parameter-input estimation results can be further used for damage diagnosis and fatigue life prediction. The calibrated model together with estimated input loads provide accurate prediction of strain/stress time histories at fatigue hotspots. This can be used to predict and assess the fatigue life of the structure, using well-established methods such as rainflow-counting algorithm, S-N curves, and Miner's rule [73]. Monitoring the structure over a longer period (e.g., several seasons) will also

provide the trends in seasonal loads which are needed when extrapolating the future loads on the structure for estimating its fatigue life.

Declaration of Competing Interest

The authors declare that they have no known competing financial interests or personal relationships that could have appeared to influence the work reported in this paper.

Acknowledgements

The authors acknowledge partial support of this study by the United States National Science Foundation grant 1903972, and Massachusetts Clean Energy Center under AmplifyMass program. The work presented was also partially supported by the INTERREG 5A Germany-Denmark program, with funding from the European Fund for Regional Development. The authors would also like to extend their gratitude to the Federal Marine and Hydrographic Agency (BSH) for providing relevant environmental data used in this study. The opinions, findings, and conclusions expressed in this paper are those of the authors and do not necessarily represent the views of the sponsors and organizations involved in this project.

References

- [1] C. Röckmann, S. Lagerveld, J. Stavenuiter, Operation and maintenance costs of offshore wind farms and potential multi-use platforms in the Dutch North Sea, in: *Aquaculture Perspective of Multi-Use Sites in the Open Ocean*, Springer, Cham, 2017, pp. 97–113.
- [2] S.P. Tchomodanova, M. Sanayei, B. Moaveni, K. Tatsis, E. Chatzi, *Strain predictions at unmeasured locations of a substructure using sparse response-only vibration measurements*, *Journal of Civil, Structural Health Monitoring* 11 (4) (2021) 1113–1136.
- [3] Y. Chen, P. Avitabile, J. Dodson, Data consistency assessment function (DCAF), *Mechanical Systems and Signal Processing* 141 (2020), 106688.
- [4] Y. Chen, P. Avitabile, C. Page, J. Dodson, A polynomial based dynamic expansion and data consistency assessment and modification for cylindrical shell structures, *Mechanical Systems and Signal Processing* 154 (2021), 107574.
- [5] Hjelm, H.P., R. Brincker, J. Graugaard-Jensen, and K. Munch. Determination of stress histories in structures by natural input modal analysis. in *Proceedings of 23rd Conference and Exposition on Structural Dynamics (IMACXXIII)*. 2005. Citeseer.
- [6] P. Avitabile, P. Pingle, Prediction of full field dynamic strain from limited sets of measured data, *Shock and vibration* 19 (5) (2012) 765–785.
- [7] C. Papadimitriou, C.-P. Fritzen, P. Kraemer, E. Ntotsios, Fatigue predictions in entire body of metallic structures from a limited number of vibration sensors using Kalman filtering, *Structural Control and Health Monitoring* 18 (5) (2011) 554–573.
- [8] A. Iliopoulos, R. Shirzadeh, W. Weijtjens, P. Guillaume, D.V. Hemelrijck, C. Devriendt, A modal decomposition and expansion approach for prediction of dynamic responses on a monopile offshore wind turbine using a limited number of vibration sensors, *Mechanical Systems and Signal Processing* 68–69 (2016) 84–104.
- [9] A. Iliopoulos, W. Weijtjens, D. Van Hemelrijck, C. Devriendt, Fatigue assessment of offshore wind turbines on monopile foundations using multi-band modal expansion, *Wind Energy* 20 (8) (2017) 1463–1479.
- [10] K. Maes, A. Iliopoulos, W. Weijtjens, C. Devriendt, G. Lombaert, Dynamic strain estimation for fatigue assessment of an offshore monopile wind turbine using filtering and modal expansion algorithms, *Mechanical Systems and Signal Processing* 76–77 (2016) 592–611.
- [11] A. Skafte, J. Kristoffersen, J. Vestermark, U.T. Tygesen, R. Brincker, Experimental study of strain prediction on wave induced structures using modal decomposition and quasi static Ritz vectors, *Engineering Structures* 136 (2017) 261–276.
- [12] M. Henkel, J. Häfele, W. Weijtjens, C. Devriendt, C. Gebhardt, R. Rolfes, Strain estimation for offshore wind turbines with jacket substructures using dual-band modal expansion, *Marine Structures* 71 (2020), 102731.
- [13] M. Tarpø, B. Nabuco, C. Georgakis, R. Brincker, Expansion of experimental mode shape from operational modal analysis and virtual sensing for fatigue analysis using the modal expansion method, *International Journal of Fatigue* 130 (2020), 105280.
- [14] D. Giagopoulos, A. Arailopoulos, V. Dertimanis, C. Papadimitriou, E. Chatzi, K. Grompanopoulos, Structural health monitoring and fatigue damage estimation using vibration measurements and finite element model updating, *Structural Health Monitoring* 18 (4) (2019) 1189–1206.
- [15] J. Kullaa, Bayesian virtual sensing in structural dynamics, *Mechanical Systems and Signal Processing* 115 (2019) 497–513.
- [16] Q.W. Zhang, T.Y.P. Chang, C.C. Chang, Finite-element model updating for the Kap Shui Mun cable-stayed bridge, *Journal of Bridge Engineering* 6 (4) (2001) 285–293.
- [17] J.M.W. Brownjohn, P. Moyo, P. Omenzetter, Y. Lu, Assessment of highway bridge upgrading by dynamic testing and finite-element model updating, *Journal of Bridge Engineering* 8 (3) (2003) 162–172.
- [18] A. Teughels, G. De Roeck, Structural damage identification of the highway bridge Z24 by FE model updating, *Journal of Sound and Vibration* 278 (3) (2004) 589–610.
- [19] B. Jaishi, H.-J. Kim, M.K. Kim, W.-X. Ren, S.-H. Lee, Finite element model updating of concrete-filled steel tubular arch bridge under operational condition using modal flexibility, *Mechanical Systems and Signal Processing* 21 (6) (2007) 2406–2426.
- [20] E. Reynders, G.D. Roeck, P. Gunders Bakir, C. Sauvage, Damage identification on the Tilff Bridge by vibration monitoring using optical fiber strain sensors, *Journal of engineering mechanics* 133 (2) (2007) 185–193.
- [21] S.-E. Fang, R. Perera, G. De Roeck, Damage identification of a reinforced concrete frame by finite element model updating using damage parameterization, *Journal of Sound and Vibration* 313 (3–5) (2008) 544–559.
- [22] B. Moaveni, A. Stavridis, G. Lombaert, J.P. Conte, P.B. Shing, Finite-element model updating for assessment of progressive damage in a 3-story infilled RC frame, *Journal of Structural Engineering* 139 (10) (2013) 1665–1674.
- [23] M. Song, S. Yousefianmoghadam, M.-E. Mohammadi, B. Moaveni, A. Stavridis, R.L. Wood, An application of finite element model updating for damage assessment of a two-story reinforced concrete building and comparison with lidar, *Structural Health Monitoring* 17 (5) (2018) 1129–1150.
- [24] J.L. Beck, L.S. Katafygiotis, Updating models and their uncertainties. I: Bayesian statistical framework, *Journal of Engineering Mechanics* 124 (4) (1998) 455–461.
- [25] K.-V. Yuen (Ed.), *Bayesian Methods for Structural Dynamics and Civil Engineering*, John Wiley & Sons, Ltd, Chichester, UK, 2010.
- [26] E. Ntotsios, C. Papadimitriou, P. Panetos, G. Karaiskos, K. Perros, P.C. Perdikaris, Bridge health monitoring system based on vibration measurements, *Bulletin of Earthquake Engineering* 7 (2) (2009) 469–483.
- [27] H.-F. Lam, J. Yang, S.-K. Au, Bayesian model updating of a coupled-slab system using field test data utilizing an enhanced Markov chain Monte Carlo simulation algorithm, *Engineering Structures* 102 (2015) 144–155.
- [28] E. Simoen, G. De Roeck, G. Lombaert, Dealing with uncertainty in model updating for damage assessment: A review, *Mechanical Systems and Signal Processing* 56–57 (2015) 123–149.
- [29] M. Song, L. Renson, J.-P. Noël, B. Moaveni, G. Kerschen, Bayesian model updating of nonlinear systems using nonlinear normal modes, *Structural Control and Health Monitoring* 25 (12) (2018), <https://doi.org/10.1002/stc.v25.1210.1002/stc.2258>.

- [30] G. Sevieri, M. Andreini, A. De Falco, H.G. Matthies, Concrete gravity dams model parameters updating using static measurements, *Engineering Structures* 196 (2019), 109231.
- [31] M. Song, B. Moaveni, C. Papadimitriou, A. Stavridis, Accounting for amplitude of excitation in model updating through a hierarchical Bayesian approach: Application to a two-story reinforced concrete building, *Mechanical Systems and Signal Processing* 123 (2019) 68–83.
- [32] Wu, M. and A.W. Smyth, *Application of the unscented Kalman filter for real-time nonlinear structural system identification*. Structural Control and Health Monitoring: The Official Journal of the International Association for Structural Control and Monitoring and of the European Association for the Control of Structures, 2007. 14(7): p. 971–990.
- [33] H. Ebrahimian, R. Astroza, J.P. Conte, Extended Kalman filter for material parameter estimation in nonlinear structural finite element models using direct differentiation method, *Earthquake Engineering & Structural Dynamics* 44 (10) (2015) 1495–1522.
- [34] Chatzi, E.N. and A.W. Smyth, The unscented Kalman filter and particle filter methods for nonlinear structural system identification with non-collocated heterogeneous sensing. Structural Control and Health Monitoring: The Official Journal of the International Association for Structural Control and Monitoring and of the European Association for the Control of Structures, 2009. 16(1): p. 99–123.
- [35] S. Eftekhar Azam, S. Mariani, Dual estimation of partially observed nonlinear structural systems: A particle filter approach, *Mechanics Research Communications* 46 (2012) 54–61.
- [36] R. Astroza, H. Ebrahimian, J.P. Conte, Material parameter identification in distributed plasticity FE models of frame-type structures using nonlinear stochastic filtering, *Journal of Engineering Mechanics* 141 (5) (2015) 04014149, [https://doi.org/10.1061/\(ASCE\)EM.1943-7889.0000851](https://doi.org/10.1061/(ASCE)EM.1943-7889.0000851).
- [37] R. Astroza, H. Ebrahimian, Y. Li, J.P. Conte, Bayesian nonlinear structural FE model and seismic input identification for damage assessment of civil structures, *Mechanical Systems and Signal Processing* 93 (2017) 661–687.
- [38] R. Astroza, A. Alessandri, Effects of model uncertainty in nonlinear structural finite element model updating by numerical simulation of building structures, *Structural Control and Health Monitoring* 26 (3) (2019) e2297, <https://doi.org/10.1002/stc.2297>.
- [39] M. Song, R. Astroza, H. Ebrahimian, B. Moaveni, C. Papadimitriou, Adaptive Kalman filters for nonlinear finite element model updating, *Mechanical Systems and Signal Processing* 143 (2020), 106837.
- [40] K. Erazo, B. Moaveni, S. Nagarajaiah, Bayesian seismic strong-motion response and damage estimation with application to a full-scale seven story shear wall structure, *Engineering Structures* 186 (2019) 146–160.
- [41] J. Sanchez, H. Benaroya, Review of force reconstruction techniques, *Journal of Sound and Vibration* 333 (14) (2014) 2999–3018.
- [42] E. Lourens, E. Reynders, G. De Roeck, G. Degrande, G. Lombaert, An augmented Kalman filter for force identification in structural dynamics, *Mechanical Systems and Signal Processing* 27 (2012) 446–460.
- [43] E. Lourens, C. Papadimitriou, S. Gillijns, E. Reynders, G. De Roeck, G. Lombaert, Joint input-response estimation for structural systems based on reduced-order models and vibration data from a limited number of sensors, *Mechanical Systems and Signal Processing* 29 (2012) 310–327.
- [44] S. Gillijns, B. De Moor, Unbiased minimum-variance input and state estimation for linear discrete-time systems with direct feedthrough, *Automatica* 43 (5) (2007) 934–937.
- [45] L. Liu, Y. Su, J. Zhu, Y. Lei, Data fusion based EKF-UI for real-time simultaneous identification of structural systems and unknown external inputs, *Measurement* 88 (2016) 456–467.
- [46] S. Eftekhar Azam, E. Chatzi, C. Papadimitriou, A dual Kalman filter approach for state estimation via output-only acceleration measurements, *Mechanical Systems and Signal Processing* 60–61 (2015) 866–886.
- [47] S.E. Azam, E. Chatzi, C. Papadimitriou, A. Smyth, Experimental validation of the Kalman-type filters for online and real-time state and input estimation, *Journal of vibration and control* 23 (15) (2017) 2494–2519.
- [48] E. Zhang, J. Antoni, P. Feissel, Bayesian force reconstruction with an uncertain model, *Journal of Sound and Vibration* 331 (4) (2012) 798–814.
- [49] H. Ebrahimian, R. Astroza, J.P. Conte, C. Papadimitriou, Bayesian optimal estimation for output-only nonlinear system and damage identification of civil structures, *Structural Control and Health Monitoring* 25 (4) (2018) e2128, <https://doi.org/10.1002/stc.v25.410.1002/stc.2128>.
- [50] M.-S. Nabiyan, F. Khoshnoudian, B. Moaveni, H. Ebrahimian, Mechanics-based model updating for identification and virtual sensing of an offshore wind turbine using sparse measurements, *Structural Control and Health Monitoring* 28 (2) (2021), <https://doi.org/10.1002/stc.v28.210.1002/stc.2647>.
- [51] F. Naets, J. Croes, W. Desmet, An online coupled state/input/parameter estimation approach for structural dynamics, *Computer Methods in Applied Mechanics and Engineering* 283 (2015) 1167–1188.
- [52] T. Pahn, R. Rolles, J. Jonkman, Inverse load calculation procedure for offshore wind turbines and application to a 5-MW wind turbine support structure, *Wind Energy* 20 (7) (2017) 1171–1186.
- [53] K.E. Tatsis, V.K. Dertimanis, C. Papadimitriou, E. Lourens, E.N. Chatzi, A general substructure-based framework for input-state estimation using limited output measurements, *Mechanical Systems and Signal Processing* 150 (2021), 107223.
- [54] R. Mehra, Approaches to adaptive filtering, *IEEE Transactions on automatic control* 17 (5) (1972) 693–698.
- [55] A. Almagbile, J. Wang, W. Ding, Evaluating the performances of adaptive Kalman filter methods in GPS/INS integration, *Journal of Global Positioning Systems* 9 (1) (2010) 33–40.
- [56] S. Akhlaghi, N. Zhou, Z. Huang, Adaptive adjustment of noise covariance in Kalman filter for dynamic state estimation, *IEEE*, 2017.
- [57] S.J. Julier, J.K. Uhlmann, H.F. Durrant-Whyte, A new approach for filtering nonlinear systems, *IEEE*, 1995.
- [58] Julier, S.J. *The scaled unscented transformation*. in *American Control Conference, 2002. Proceedings of the 2002*. 2002. IEEE.
- [59] B. Moaveni, X. He, J.P. Conte, J.I. Restrepo, Damage identification study of a seven-story full-scale building slice tested on the UCSD-NEES shake table, *Structural Safety* 32 (5) (2010) 347–356.
- [60] Chandrupatla, T.R., A.D. Belegundu, T. Ramesh, and C. Ray, *Introduction to finite elements in engineering*. Vol. 10. 2002: Prentice Hall Upper Saddle River, NJ.
- [61] *FINO3 – research platform in the North Sea and the Baltic No. 3*. Available from: <https://www.fino3.de/en/>.
- [62] *OpenSees 2.5.0*. University of California, Berkeley.
- [63] L. Arany, S. Bhattacharya, S. Adhikari, S.J. Hogan, J.H.G. Macdonald, An analytical model to predict the natural frequency of offshore wind turbines on three-spring flexible foundations using two different beam models, *Soil Dynamics and Earthquake Engineering* 74 (2015) 40–45.
- [64] S. Bhattacharya (Ed.), *Design of Foundations for Offshore Wind Turbines*, Wiley, 2019.
- [65] D.N. Veritas, *Offshore Standard DNV-OS-J101: Design of Offshore Wind Turbine Structures*, Det Norske Veritas, Høvik, Norway, 2004.
- [66] IEC, *International Standard IEC-61400-1 Wind Turbines – Part 1: Design requirements*. 2005, IEC.
- [67] ASCE. *Minimum design loads for buildings and other structures*. 2013. American Society of Civil Engineers.
- [68] Van Overschee, P. and B. De Moor, *Subspace identification for linear systems: Theory—Implementation—Applications*. 2012: Springer Science & Business Media.
- [69] Peeters, B., System identification and damage detection in civil engineering. 2000.
- [70] P. Moser, B. Moaveni, Design and deployment of a continuous monitoring system for the Dowling Hall Footbridges, *Experimental Techniques* 37 (1) (2013) 15–26.
- [71] *MATLAB*. MathWorks.
- [72] R. Astroza, A. Alessandri, J.P. Conte, A dual adaptive filtering approach for nonlinear finite element model updating accounting for modeling uncertainty, *Mechanical Systems and Signal Processing* 115 (2019) 782–800.
- [73] M.A. Miner, Cumulative Damage in Fatigue, *Cumulative damage in fatigue*. 12 (3) (1945) A159–A164.